# MARS GLOBAL SURVEYOR MEASUREMENTS OF THE MARTIAN SOLAR WIND INTERACTION

D. A. BRAIN
*University of California, Berkeley Space Sciences Laboratory, Berkeley, CA 94720*
*(E-mail: brain@ssl.berkeley.edu)*

(Received 8 August 2006; Accepted in final form 17 November 2006)

**Abstract.** The solar wind at Mars interacts with the extended atmosphere and small-scale crustal magnetic fields. This interaction shares elements with a variety of solar system bodies, and has direct bearing on studies of the long-term evolution of the Martian atmosphere, the structure of the upper atmosphere, and fundamental plasma processes. The magnetometer (MAG) and electron reflectometer (ER) on Mars Global Surveyor (MGS) continue to make many contributions toward understanding the plasma environment, thanks in large part to a spacecraft orbit that had low periapsis, had good coverage of the interaction region, and has been long-lived in its mapping orbit. The crustal magnetic fields discovered using MGS data perturb plasma boundaries on timescales associated with Mars' rotation and enable a complex magnetic field topology near the planet. Every portion of the plasma environment has been sampled by MGS, confirming previous measurements and making new discoveries in each region. The entire system is highly variable, and responds to changes in solar EUV flux, upstream pressure, IMF direction, and the orientation of Mars with respect to the Sun and solar wind flow. New insights from MGS should come from future analysis of new and existing data, as well as multi-spacecraft observations.

**Keywords:** Mars, MGS, magnetosphere, solar wind interaction

## 1. Introduction

The Martian interaction with the solar wind provides an interesting contrast to the plasma interactions at other solar system bodies. The solar wind obstacle is a combination of a global atmospheric obstacle (like those at Venus or comets) punctuated by many smaller-scale obstacles formed by strong crustal magnetic fields (similar, perhaps, to Earth or the Moon). The supersonic solar wind evolves in density, temperature, and the strength of its entrained Interplanetary Magnetic Field (IMF) as it expands into the solar system, so that the incident plasma at Mars has properties intermediate between those experienced by the inner and outer planets.

In addition to being of general interest, the plasma environment influences at least three "big picture" science issues. First, studies of the Martian solar wind interaction provide important contributions toward understanding the long-term evolution of the Martian climate since the end of the late heavy bombardment. A variety of lines of evidence suggest that the Martian atmosphere has been substantially altered

Space Science Reviews (2006) 126: 77–112
DOI: 10.1007/s11214-006-9122-x

over time (see Jakosky and Phillips, 2001). Escape of atmospheric particles to space is known to occur in the present epoch (e.g. Lundin *et al.*, 1989; Carlsson *et al.*, 2006), and likely has been the most efficient loss process over the last 3.5 billion years or more (Brain and Jakosky, 1998). Of the variety of physical processes collectively termed 'escape to space', all ion loss processes are directly influenced by the solar wind plasma and magnetic field, as is the loss of neutrals via 'sputtering' by pickup ions (and the upper atmospheric reservoir for escaping neutrals). Second, the solar wind provides a boundary condition for the current state of the upper atmosphere, and therefore plays a role in determining its structure, composition, chemistry, and dynamics. Solar wind charged particles (as well as neutrals formed in the solar wind via charge exchange) have access to the thermosphere at low altitudes (Mitchell *et al.*, 2001a), and can contribute to atmospheric energy deposition and ionization. Sharp contrasts in structure and composition can develop near crustal field boundaries (Gurnett *et al.*, 2005), driving dynamics. The Martian upper atmosphere would be remarkably different without the plasma interaction, which is therefore a necessary component in its understanding. Finally, Mars offers a natural laboratory for exploration of fundamental plasma processes observed at Earth and elsewhere in the solar system and universe. Processes such as particle acceleration, magnetic reconnection or merging, and the generation of instabilities in the form of plasma waves and shocks all occur at Mars in plasma conditions that differ significantly from those observed elsewhere. Mars has the potential to provide a useful end-member data point on how these processes operate.

The main features of the Martian global plasma interaction are summarized in cartoon form in Figure 1. Solar wind ions (indicated in blue) and the associated interplanetary magnetic field (IMF) interact with the extended Martian atmosphere (indicated in orange) and ionosphere. A variety of different plasma regimes and boundaries form as a result, and can be distinguished using spacecraft particle and field measurements. The solar wind transitions from supersonic to subsonic as it crosses the bow shock into the hotter, denser, more turbulent magnetosheath. Some solar wind plasma is reflected from the shock into the foreshock region. Few or no solar wind protons are observed downstream from a boundary sometimes called the magnetic pile-up boundary (or MPB) and its tailward extension (however the shocked IMF and solar wind electrons are found downstream from this boundary, presenting a challenge in interpretation). Below the MPB, the photoelectron boundary (PEB) separates the planetary ionosphere from the magnetic pileup region (MPR). A two-lobed induced magnetotail forms on the night side, with a current sheet carrying planetary ions between the two lobes. Crustal remnant magnetic fields perturb the global interaction at low altitudes.

What is known about the Martian solar wind interaction has been derived primarily from measurements made by spacecraft missions to Mars over the past 40 years. Historical spacecraft measurements are described in several review articles (e.g. Luhmann *et al.*, 1992; Barabash and Lundin, 2006); the main contributions are summarized here. Equipped with a magnetometer, the Mariner 4 spacecraft made

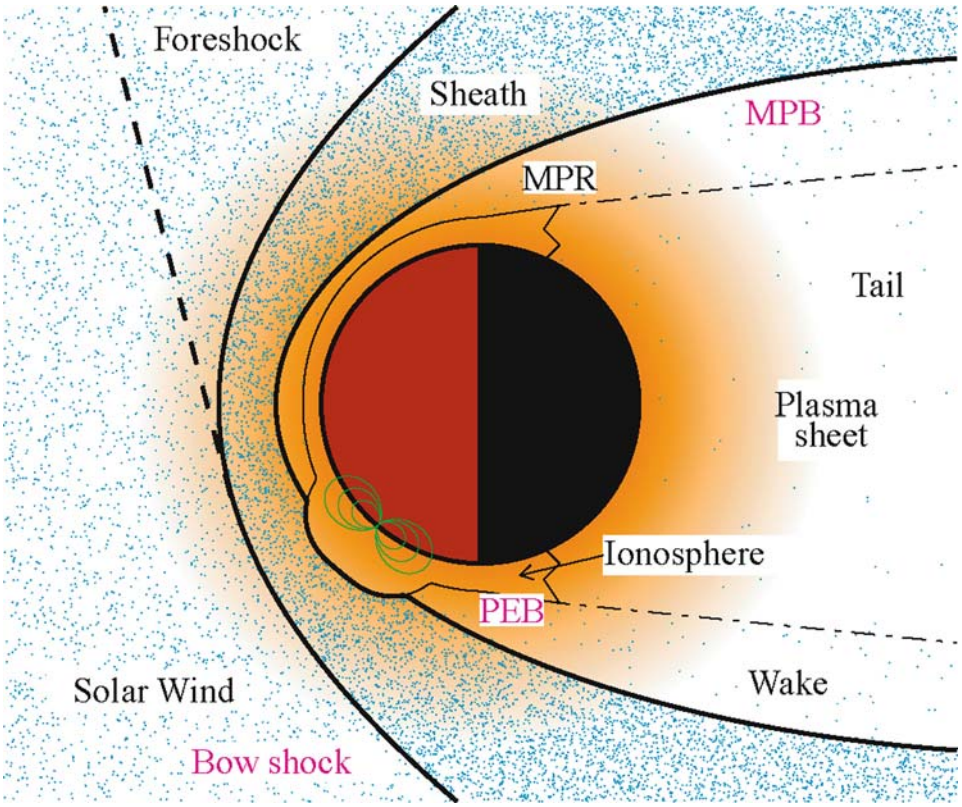


*Figure 1*. Cartoon of the global Martian solar wind interaction. Orange shading indicates density of planetary neutrals. Blue indicates relative density of solar wind ions in different plasma regions (labeled in black), separated by different plasma boundaries (labeled in magenta). Boundary names in this figure are those specific to MGS literature.

the first measurements of a non-terrestrial bow shock on two flybys in July 1965 (Smith, 1969). From 1971 to 1974 the Soviet Mars missions (2, 3, 5) also measured the bow shock and the underlying sheath using magnetometers and ion and electron instruments (e.g. Bogdanov and Vaisberg, 1975; Dolginov *et al*., 1976). Additionally, they made the first measurements of the "ion cushion", identified in Figure 1 as the MPR. There were no more measurements of the plasma interaction at Mars until the arrival of the Phobos 2 spacecraft in 1989, though the Viking 1 and 2 Landers in 1976 measured *in situ* vertical density and temperature profiles in the ionosphere (Hanson *et al*., 1977). Phobos 2 measured escape products from the Martian atmosphere, and provided a wealth of useful information about the Martian wake, tail, sheath, and upstream regions (e.g. Lundin *et al*., 1989; Riedler *et al*., 1989; Rosenbauer *et al*., 1989; Pedersen *et al*., 1991; Verigin *et al*., 1991, 1993; Dubinin *et al*., 1993, 1994, 1996). Mars Global Surveyor (MGS), discussed in this review, discovered strong crustal magnetic fields that interact directly with the

shocked solar wind, and placed a new upper limit on the strength of any lingering Martian dynamo (Acuña *et al*., 1998, 2001). The Mars Express (MEX) spacecraft, in orbit since late 2003, has made the first low-altitude measurements of planetary heavy ions (Lundin *et al*., 2004), the first measurements of Energetic Neutral Atoms (ENAs) at Mars (Futaana *et al*., 2006), and has discovered aurora in the crustal magnetic fields (Bertaux *et al*., 2005). At the time of this review there is considerable opportunity for new discovery. Both MGS and MEX continue to operate and make new measurements, Venus Express is making measurements at Venus that can be directly compared to MEX data, and several new spacecraft missions are being considered or proposed.

Previous review papers have been published on many of the spacecraft missions and results described above. These include reviews of Phobos results (Zakharov, 1992), Mars Express results (Barabash and Lundin, 2006), subsets of the MGS results (Crider, 2004; Bertucci *et al*., 2005a), and reviews of the Martian system that are not specific to any one spacecraft (e.g. Nagy *et al*., 2004; Luhmann *et al*., 1992). The purpose of this review is to illustrate the unique contributions of the MGS mission to the study of the Martian interaction with the solar wind, incorporating recent results and highlighting opportunities for future discoveries. In the sections that follow we will describe the MGS instrument suite and orbit (Section 2), and MGS contributions related to the crustal magnetic fields (Section 3), global solar wind interaction (Section 4), and variability (Section 5). We follow with a brief summary (Section 6) and directions for the future.

## 2. MGS Measurements

### 2.1. Instrumentation

MGS carries three instruments capable of returning information about the solar wind interaction with the upper atmosphere: a magnetometer (MAG), an electron reflectometer (ER), and a radio science investigation (RS).

MAG consists of two triaxial fluxgate magnetometers mounted on the spacecraft solar panels. MAG returns full vector magnetic field measurements every 0.75–3 s, and successive vector field differences 24 times as often. The instrument has dynamic range of 0.005–65536 nT. The instrument was calibrated in-flight to remove spacecraft-generated magnetic fields, and is accurate to $\sim 1$ nT (Acuña *et al*., 2001). As of early 2006, MAG has returned more than 4.2 billion vectors from the Martian system. Further details about the instrument can be found in Acuña *et al*. (1992, 1998). Previous spacecraft to carry magnetometers to Mars include Phobos, Mars 2, 3, and 5, and Mariner 4.

ER is a top-hat electrostatic analyzer designed to measure fluxes of superthermal electrons in a planar slice through the 3D distribution. Full 3D electron distributions are not measured because the MGS spacecraft is three-axis stabilized. Directional

information in energy channels ranging from 10 eV to 20 keV is obtained every 2–8 seconds from 16 sectors measuring 14° by 22.5°. Omni-directional energy spectra with 25% energy resolution are recorded every 12–48 seconds. More information on the MGS ER can be found in Acuña *et al.* (1992); Mitchell *et al.* (2001a). The Phobos and Mars 5 spacecraft carried instruments capable of measuring electrons prior to the arrival of MGS, and MEX also carries an electron sensor.

The MGS radio science (RS) investigation returns information relevant to the solar wind interaction in the form of upper atmospheric electron density profiles derived from radio occultations (Tyler *et al.*, 2001; Hinson *et al.*, 1999). Details about the RS instrument can be found in Tyler *et al.* (1992). The MGS RS investigation has returned many more profiles than previous missions, combined. RS results will not be discussed in detail in this review. Major results include identification of different ionospheric scale heights in the vicinity of crustal magnetic sources (Krymskii *et al.*, 2004), identification of "anomalous" electron density profiles in the vicinity of crustal magnetic fields (Withers *et al.*, 2005), measurement of enhancements in ionospheric densities due to solar flares (Mendillo *et al.*, 2006), and measurement of simultaneous variability in the ionospheres of Mars and Earth (Mendillo *et al.*, 2003). Ionospheric measurements at Mars prior to MGS are summarized in Mendillo *et al.* (2003).

## 2.2. Orbit

In some respects, the many contributions of the MAG/ER to the study of the Martian solar wind interaction were made possible by the unique orbit of the MGS spacecraft. The mission had two main phases – premapping and mapping, also described in Albee *et al.* (2001).

The first phase, premapping, lasted from 13 September 1997 through late January 1999. During this time period MGS had an elliptical orbit that precessed in local time and gradually circularized, with periapsis as low as ∼101 km and apoapsis as high as ∼16 Mars radii ($R_M$). MGS was actively aerobraking in the Martian atmosphere during some of these orbits, and was in a "holding" orbit at other times as it precessed to the local time for the mapping orbit. Figure 2 shows the orbital coverage of low altitude MAG data as a function of altitude, planetary latitude, solar zenith angle, and local time. Overall, the data coverage is unprecedented at all altitudes. Data coverage is uniform in planetary longitude. There is good altitude coverage as a function of latitude, though much of the lowest altitude data north of 60° S were recorded when MGS was in sunlight. Coverage is poor near the dawn terminator, and the subsolar and anti-solar points. Further, it is apparent from the figure that solar zenith angle coverage is convolved with both latitude and local time, making it difficult to exclusively identify trends in the observations as being associated with one parameter. Finally, most of the local time coverage occurred when MGS had periapsis in the northern hemisphere.

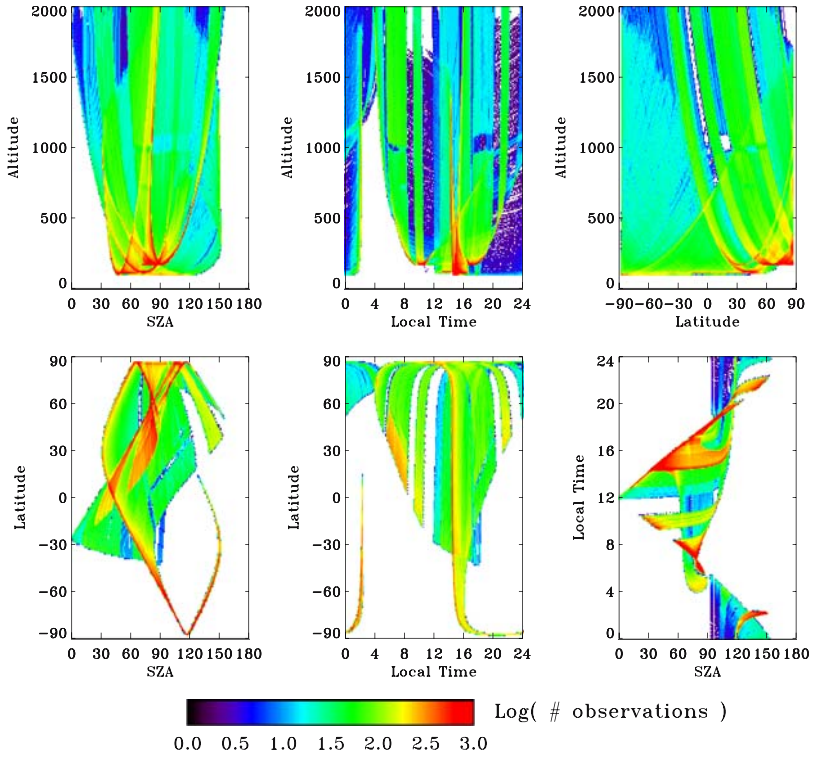


*Figure 2.* Data coverage for MGS MAG full vector measurements recorded during premapping orbits from 13 September 1997 through 28 January 1999. Panels show data density for times when the spacecraft was below 2000 km altitudes, as a function of altitude, solar zenith angle, local time, and latitude.

Since mid-1999, MGS has been in a nearly circular mapping orbit with fixed local time near 2am/2pm. The spacecraft altitude ranges from ∼369–441 km, and since the periapsis latitude is very near −90° latitude, altitude and latitude covary. Figure 3 shows the analogue of Figure 2 for the mapping orbits. All parameters are convolved during mapping, though the seasonal orientation of Mars with respect to the Sun allows some solar zenith angle coverage at certain altitudes, latitudes, and local times.

Three features of the MGS orbit enabled it to make important contributions not possible using earlier spacecraft:

1. *Low altitude* – The low periapsis altitude of the premapping orbits allowed one of the most significant discoveries of the MGS mission – the detection of Mars' crustal magnetic fields. Though Phobos approached to within ∼800 km of the planet, low enough to measure the strongest crustal field signatures over a small region of the southern hemisphere (Brain *et al.*, 2003), unambiguous association

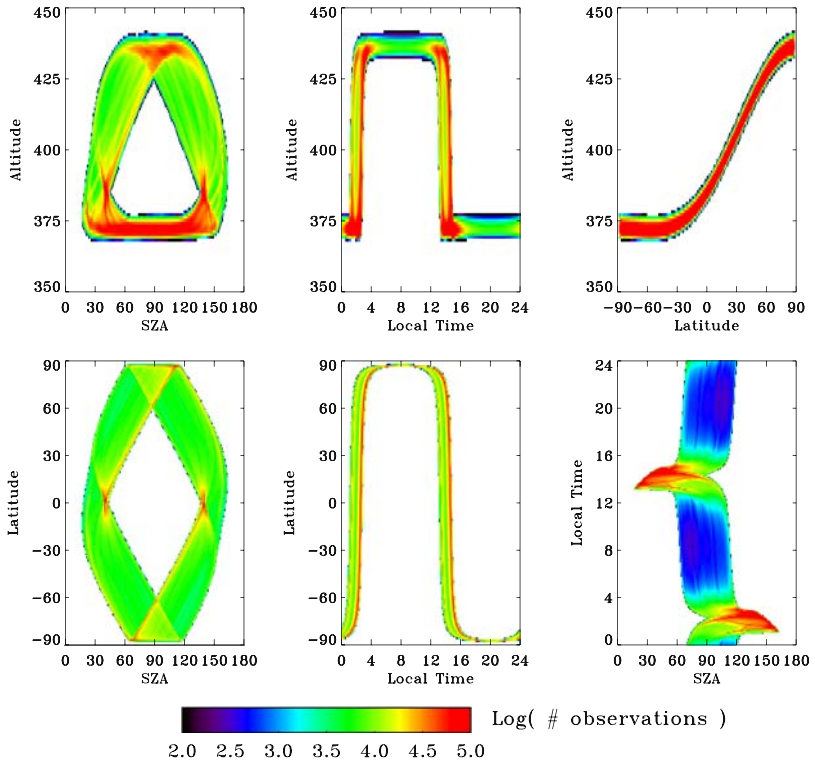


*Figure 3*. Data coverage for MGS MAG during mapping orbits from 2 June 1999 and 31 March 2004, in the same format as Figure 2.

of these signatures with crustal fields would have been very difficult without supporting data from lower altitudes.

2. *Global coverage* – The long duration of the premapping phase of the MGS mission, made necessary by a possible problem with a hinge on one of the solar panels (Albee *et al*., 2001), was a boon for the MAG/ER experiment. MGS achieved much better coverage of the global interaction region than it would have otherwise, and much better coverage than any previous spacecraft to visit Mars. Each of the regions identified in Figure 1 was visited at a variety of local times and solar zenith angles by MGS.
3. *Long-lived mapping orbit* – MGS has been in its mapping orbit for more than three Martian years, making repeated measurements of a small slice of the global interaction region. The long baseline of observations enables investigation of the many factors that control variability in this slice over timescales ranging in length from hours to a solar cycle.

Each of the three science consequences of the MGS orbit listed above is described in more detail in the following sections.

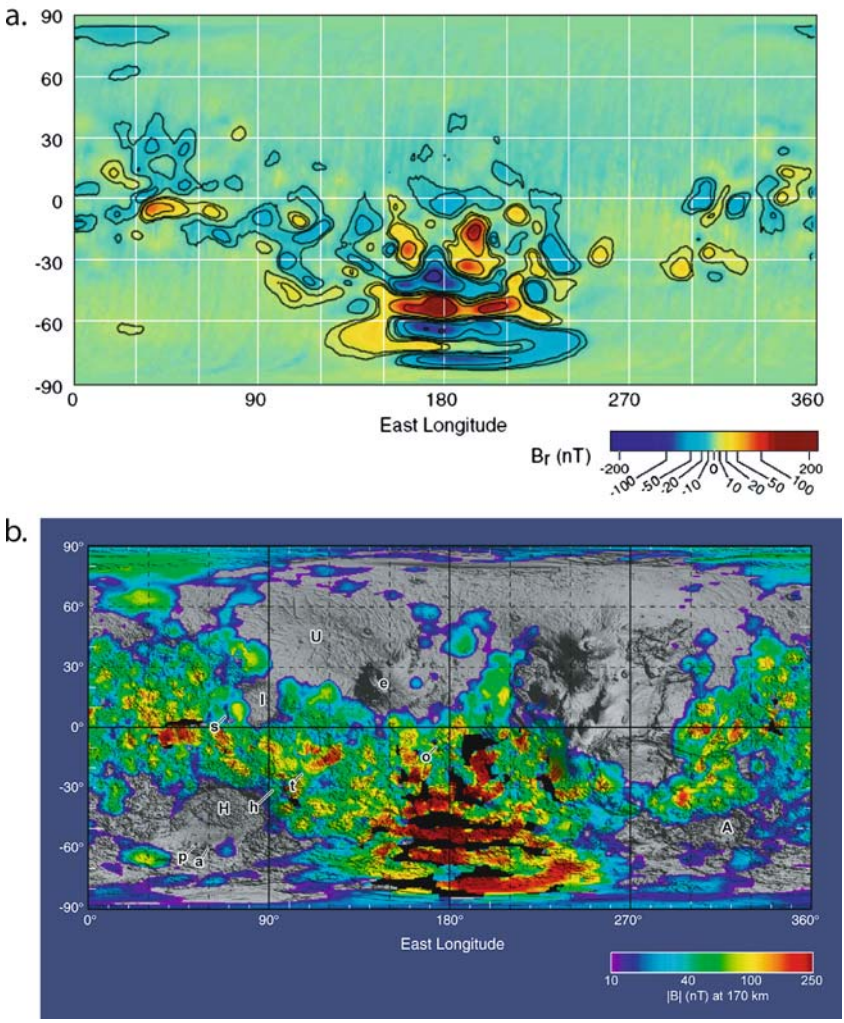


*Figure 4*. Martian crustal magnetic field maps based on MGS mapping data in eclipse. (a) Radial field component typically measured by MAG at ~400 km altitude from Connerney *et al*. (2001). (b) Field strength at 170 km altitudes inferred calculated from the shape of ER angular distributions from Mitchell *et al*. (2006).

## 3. Crustal Fields

The low periapsis of MGS allowed the discovery of crustal magnetic fields over much of the surface. Figure 4 shows that crustal fields are strongest in the heavily cratered (and therefore older) southern hemisphere, except in the locations of large impact basins such as Hellas and Argyre, which are largely devoid of enhanced magnetic fields (Acuña *et al*., 1999). The large strength of the crustal fields measured

at spacecraft altitude imply that there are large volumes of coherently magnetized material in the outer layers of the Martian crust. The most likely scenario for their formation is in the presence of a global dynamo magnetic field that has since ceased (Acuña *et al*., 1998). Even in the younger, sparsely cratered northern hemisphere there is evidence from both MAG and electron data for weaker crustal magnetic fields in some locations (Lillis *et al*., 2004; Connerney *et al*., 2005; Mitchell *et al*., 2006; Brain *et al*., 2003), with implications for the formation mechanism of the north-south dichotomy at Mars.

For reference, the largest crustal magnetic field strength measured at Mars was ∼1600 nT near 100 km altitude. The draped IMF at Mars typically reaches strengths of 30–60 nT. At the ∼400 km mapping orbit of MGS, crustal fields measure as much as 200 nT, compared to 26000 nT and 10 nT from Earth's global field and anomalies, respectively. The Martian crustal fields are also much stronger than lunar anomalies, which measure ∼30 nT at ∼20 km altitudes.

The large strength of the crustal fields also has unanticipated implications for the Martian solar wind interaction. Maps of crustal magnetic fields are created using data from the Martian nightside, in shadow, where the contributions from the draped IMF are minimized (Connerney *et al*., 2001). However, the signature of crustal fields can be measured at all solar zenith angles at Mars, and to considerable altitude. Using pre-mapping MAG data above individual regions of the surface, Brain *et al*. (2003) qualitatively determined the typical altitude to which crustal magnetic fields can be distinguished in observations. Crustal fields extend above 120 km altitude (near the ionospheric main peak) over ∼70% of the surface, and even extend above 1000 km altitudes over the strongest southern source.

The large region of influence of crustal magnetic fields adds several layers of complexity to the study of the Martian solar wind interaction. Even if all other sources of variability were held constant, the Martian interaction would be highly variable simply because the planet's rotation would change the orientation of crustal fields with respect to the solar wind. Many consequences of the crustal fields for the plasma interaction, locally and globally, have been considered. All of these effects are related to one of two influences that crustal fields have on the system: the upward perturbation of plasma boundaries, and the modification of magnetic field topology. Each effect is discussed further below.

### 3.1. Crustal Influences on Plasma Boundaries

Magnetic pressure from crustal magnetic fields can be comparable to or even far exceed ionospheric thermal pressure above selected regions of the Martian surface. This additional pressure contribution locally raises the altitude of the solar wind obstacle. The cartoon in Figure 5a illustrates that the theoretical pressure balance obstacle to the solar wind can exceed altitudes of 1200 km in some locations. This is far higher than the obstacle in the northern hemisphere, where the crustal

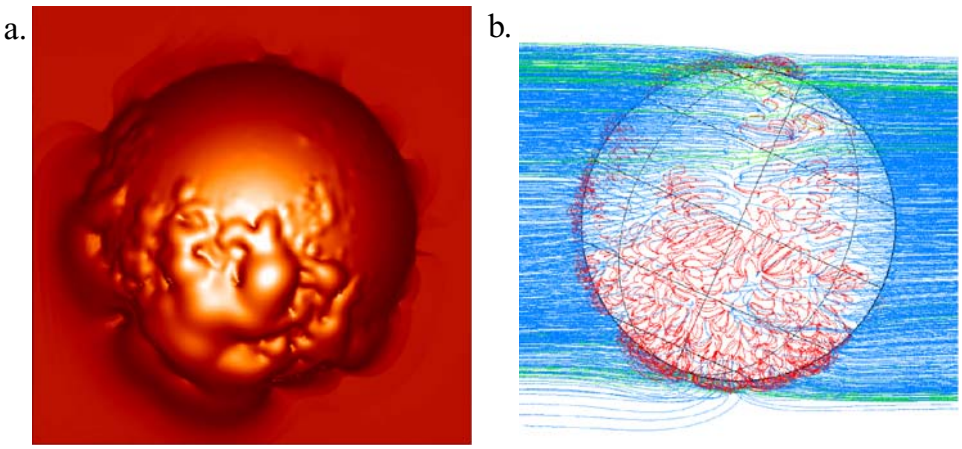


*Figure 5.* Cartoon showing: (a) the Martian pressure balance obstacle and (b) magnetic field topology. (a) The shape of the Martian solar wind obstacle is derived from a calculation of pressure balance between upstream solar wind dynamic pressure and a combination of ionospheric thermal pressure and magnetic pressure from crustal fields. (b) The magnetic field topology results from field line tracing in a vacuum superposition of a crustal field model with a uniform background magnetic field. Field lines are colored according to their topology: closed (red), open (blue), or draped (green). Mars has the same orientation in both panels. From Brain (2002).

magnetic pressure is small compared to thermal pressure contributions. Therefore, the Martian obstacle should be qualitatively similar to Earth's magnetopause in some locations, and similar to the Venus obstacle in others.

Crustal fields are known to perturb two boundaries in MGS data. The photoelectron boundary reported by (Mitchell *et al.*, 2000) is located at higher altitudes over regions of strong horizontal crustal magnetic field Mitchell *et al.* (2001b). Crustal fields prevent solar wind electrons from accessing the ionosphere in these locations, locally shielding the atmosphere so that ionospheric photoelectrons signatures are detectable by ER. Consequently, ionization processes associated with the solar wind (electron impact and charge exchange) can not occur under these protective bubbles of field, and global fluxes of escaping ions may be reduced.

At higher altitudes the MPB is also perturbed or modified by the presence of strong crustal magnetic fields. Crider *et al.* (2002) used MGS premapping orbits to show that the MPB occurs at higher altitudes in the southern hemisphere, where crustal fields are strongest (see Figure 6). Subsequently, Brain *et al.* (2005a) demonstrated using mapping orbits that, like the PEB, the MPB is higher in particular over strong horizontal crustal fields. Hall MHD model results reported by Harnett and Winglee (2003) suggest that the MPB is different above crustal fields, with more similarities to a magnetopause.

There has been no detected influence of the crustal fields on the location of the bow shock (Vignes *et al.*, 2002). One might expect a connection (e.g. Acuña *et al.*,

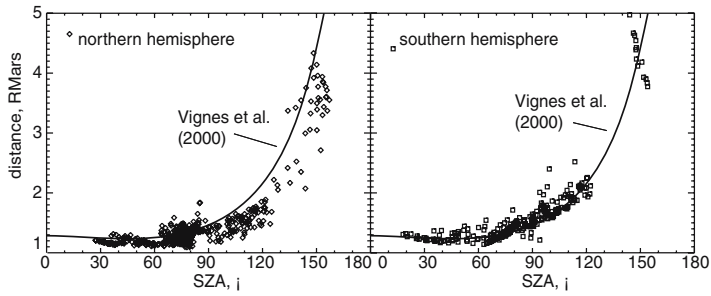


*Figure 6.* MPB crossings from MGS premapping data are plotted as a function of solar zenith angle (SZA) in the northern hemisphere (left) and southern hemisphere (right). The best-fit shape for the MPB calculated by Vignes *et al.* (2000) using all MPB crossings is shown in both panels for reference. From Crider *et al.* (2004).

1998), since the bow shock location is effectively determined by the location of the solar wind obstacle, which is surely perturbed by crustal fields. However, the bow shock occurs at much higher altitudes than the PEB or MPB, so that local effects from crustal fields may be of minor importance compared to the larger variations in bow shock location caused by external influences such as the direction of the IMF or changes in solar wind pressure (Dubinin *et al.*, 1998; Vignes *et al.*, 2002).

In addition to these local effects, crustal fields may also have global influence on the plasma interaction. There is some indication from statistical analysis of MGS mapping data that the altitude of the magnetosheath on the entire day side (even far from crustal fields) is raised during southern summer at Mars, when the strongest southern crustal fields approach subsolar latitudes (Brain *et al.*, 2005a). The interaction of the shocked solar wind with crustal fields also likely creates current systems in the ionosphere over the entire dayside (Luhmann *et al.*, 2002), creating a global ionospheric dynamo (Withers *et al.*, 2005). Finally, on the Martian nightside, the width of the induced magnetotail calculated from model fits to the dayside MPB crossings was found to be wider when strong crustal sources were beneath the MPB on the dayside (Verigin *et al.*, 2004). Additional results on the degree to which crustal fields perturb plasma boundaries near Mars are becoming available from Mars Express (see Fraenz *et al.* and Dubinin *et al.*, this issue).

### 3.2. Crustal Influences on Topology

In the absence of crustal sources the IMF would provide the only source of magnetic field at Mars (induced ionospheric magnetic fields ultimately originate from the solar wind). In this Venus-like case, all magnetic field lines, regardless of how they are configured in the Martian system, have both "ends" in the passing IMF. Crustal fields make possible a system with far greater complexity. Field lines near Mars may have one of three different topologies – closed field lines connected at both ends

to Mars (i.e. crustal field lines), unconnected field lines connected at both ends to the IMF, and open field lines connecting Mars to the IMF. Open field lines provide an additional opportunity for direct particle exchange between the solar wind and the upper atmosphere of Mars. Changes in topology via reconnection or merging enable the trapping of solar wind plasma in crustal magnetic field "umbrellas", and release of confined ionospheric plasma to the solar wind.

Several groups have considered the Martian field topology and its implications. The cartoon in Figure 5b shows magnetic field lines predicted by a simple linear superposition of the Cain *et al.* (2003) crustal field model with a uniform background "IMF". All three field topologies are present, and magnetic cusps are predicted above some of the strong crustal field regions. More closed field lines are predicted in the southern hemisphere than in the north. The topology of magnetic field near Mars is in many ways more similar to that of the Sun than any other solar system body. More sophisticated vacuum superpositions of crustal field models with an external field have been performed by Luhmann *et al.* (2002) and Brain (2002), with similar qualitative results. Global simulations that include crustal fields predict the presence of open and closed field lines for different orientations of Mars with respect to the Sun and solar wind (e.g. Ma *et al.*, 2002, 2004; Harnett and Winglee, 2005), and there is opportunity to compare these predictions to observations.

Other groups have used MGS data to identify locations having different field topologies. This has proved difficult using *in situ* observations. Krymskii *et al.* (2002a) used maps of the nightside magnetic field orientation created by Connerney *et al.* (2001), and identified locations of likely solar wind energy deposition in magnetic cusps through comparison with idealized dipoles having different orientations. As they note, the search for cusps is complicated by the fact that the orientation of a magnetic field line with respect to the surface does not necessarily dictate its topology. One can conceive of horizontal field lines that connect to cusps of open (and radial) field at lower altitudes, and radial field lines that are part of closed loops. The electron energy spectrum was used by Mitchell *et al.* (2001a) to indirectly identify closed field lines on the night side. Observations for which the measured electron fluxes were consistent with instrumental background, termed 'plasma voids', were inferred to be made on closed field lines where electron source processes are negligible. Plasma voids are observed with regularity in regions of strong horizontal crustal magnetic field (see Figure 7). Plasma voids are punctuated in MGS data by 'flux spikes' observed on radially oriented crustal field lines, where electron fluxes exceed those observed on the night side far from crustal fields. Flux spikes were taken as indicators of open magnetic field lines. Most recently, Brain *et al.* (2004) have used the shape of electron pitch-angle distributions to infer the topology of field lines visited by MGS. They find that the pitch angle distributions have characteristic shapes that can be associated with different topologies. For example, plasma voids and trapped distributions occur on closed field lines. One-sided loss cones indicate field lines where a portion of the most field-aligned incident electron flux has been partially absorbed by the atmosphere below the spacecraft; such

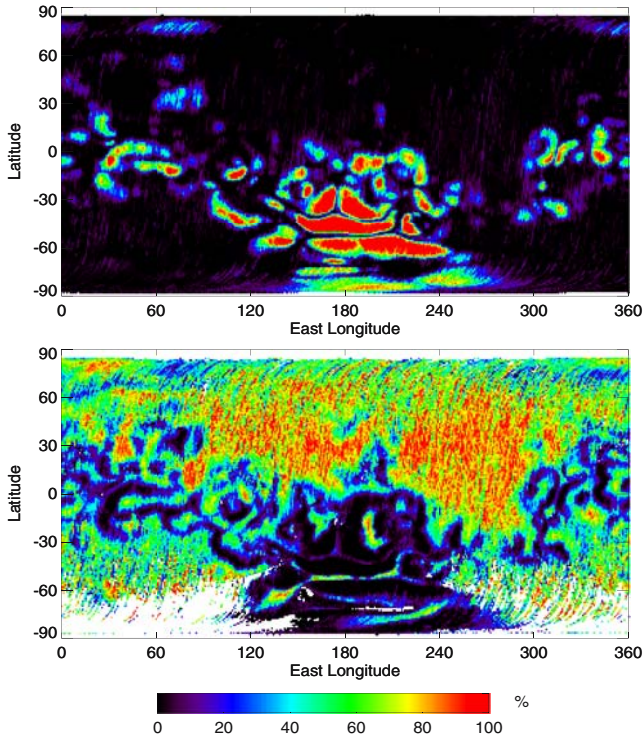


*Figure 7.* Geographic probability maps showing the location of plasma voids (top) and one-sided loss cones in ER mapping pitch angle distributions recorded in eclipse. From Brain *et al*., JGR, to be submitted.

distributions are found on open and draped field lines. This method has been used to produce maps of magnetic field topology for Mars (Figure 7), but the analysis is somewhat hampered by the 2-dimensional nature of the ER observations (which results in incomplete coverage in pitch-angle space for many observations), and has only been successfully applied to a fraction of the MGS dataset.

One specific consequence of the complex topology at Mars is the exchange of energy and particles between the upper atmosphere and solar wind (Acuña *et al*., 1998). The neutral thermospheric scale height is larger above regions of vertical magnetic field (Krymskii *et al*., 2002a), presumably because the solar wind heats the neutral atmosphere on open field lines. Cusps of open field may also allow ion outflow to occur, analogous to Earth's cusps (Lundin *et al*., 2005; Ergun *et al*., 2006). The radar sounder (MARSIS) on MEX has observed near-vertical ionization layers in the Martian atmosphere close to regions of strong radial magnetic field, as might be formed by solar wind particle and energy deposition (Nielsen *et al*., 2006). And energetic electron distributions of the type reported by Lundin *et al*. (2005); Brain *et al*. (2005b) are predicted to create localized patches of ionization on the night side (Fillingim *et al*., 2006). Finally, electrons reflected and backscattered

from the Martian nightside atmosphere along open field lines have even be used to probe neutral thermospheric densities (and map crustal magnetic field strengths) below the MGS mapping altitude (Lillis *et al*., 2004, 2005; Mitchell *et al*., 2006).

## 4. Global Interaction

Prior to MGS, Phobos was the only spacecraft to cover the Martian plasma interaction globally, and this coverage was both sparse (there were only 4 elliptical orbits and ∼100 circular orbits) and incomplete (periapsis did not go below 800 km). The elliptical premapping orbits of MGS allowed it to visit all plasma regimes in the interaction region (albeit with fewer plasma instruments), from upstream of the bow shock to the ionosphere near the main peak. It covered most of these regions over a range of solar zenith angles and local times, making new discoveries and confirming past measurements. In the following section we review highlights of the MGS contributions toward understanding the global plasma interaction.

### 4.1. Global Views

MGS observations have been used to examine the interaction in a global sense by visualizing the entire system with data. The structure of magnetic fields near Mars has been illustrated in a number of ways by different investigators. MGS confirmed that field magnitude is greatest at low altitudes and solar zenith angles, and RMS (root mean square) is greatest in the sheath between the bow shock and the MPB at low solar zenith angles (see Figure 8a and b) (Brain *et al*., 2003) . The field is draped on the day side, flares away from the planet with increasing solar zenith angle, and stretches into a two-lobed magnetotail on the night side. The flaring angle of the draped magnetic field has been treated more quantitatively by Crider *et al*. (2001), who found that the flaring of the IMF is less pronounced (but more variable) in the ionosphere than above it. Crider *et al*. (2004) showed that the average measured magnetic field as a function of location in cylindrical coordinates closely resembles the predictions of a simple gasdynamic model where the best-fit MPB was taken as the solar wind obstacle.

MAG data have also been analyzed in order to visualize the properties of electromagnetic plasma waves throughout the Martian system. Properties such as wave frequency, polarization, ellipticity, and propagation direction have been mapped in cylindrical coordinates in the Martian sheath, MPR, and tail by Espley *et al*. (2004a). Wave power at the local gyrofrequency has been mapped in the upstream region by Brain *et al*. (2002). Different wave properties dominate in different regions. Both whistler waves and waves at the local gyrofrequency are detected upstream (Brain *et al*., 2002; Mazelle *et al*., 2004), while in the sheath the observed wave properties are consistent with mirror mode waves on the day side and oscillations associated

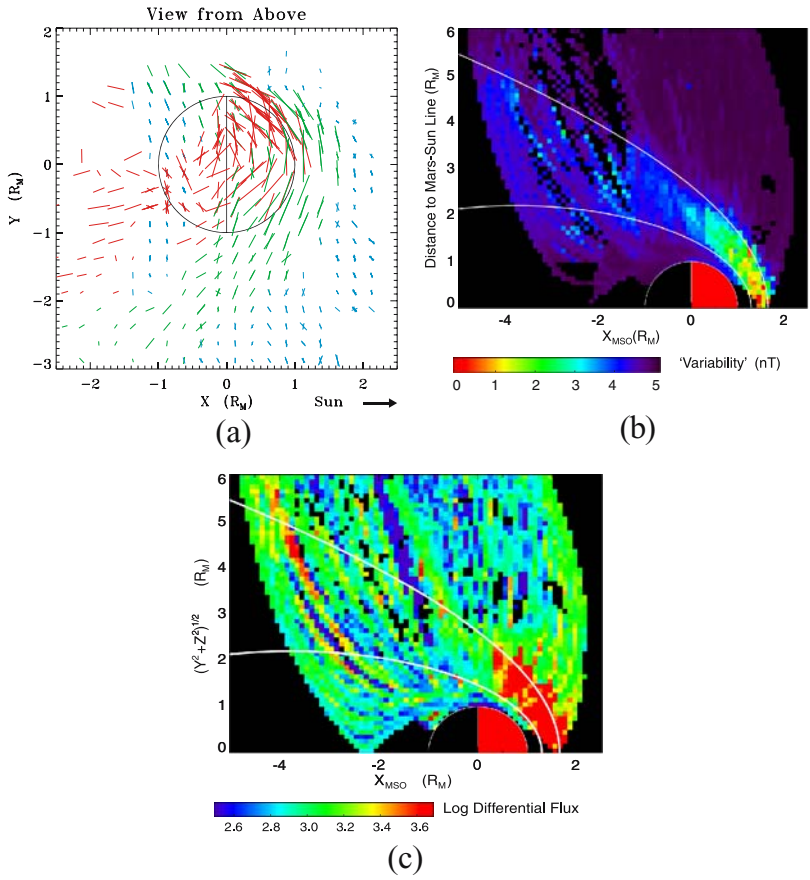


*Figure 8.* Global views in MSO cylindrical coordinates of the interaction region using MGS premapping observations. (a) Projection of median magnetic field vectors onto the $x - y$ plane, with 20 nT = 1 $R_M$. Vectors are colored according to whether they are outside the shock (blue), in the sheath(green), or below the MPB (red) as determined from the fits of Vignes *et al.* (2000). From Brain *et al.* (2003). (b) RMS noise in MAG data on 30 second timescales. From Brain *et al.* (2003). (c) Differential electron flux (#/s cm$^2$ ster eV) at 300 eV.

with the interaction of cold pickup ions with solar wind protons on the night side (Bertucci *et al.*, 2004; Espley *et al.*, 2004a). A mixture of wave modes is observed in the MPR (Espley *et al.*, 2004a), including fast mode MHD waves (Bertucci *et al.*, 2004). A mixture of wave modes is also likely to be responsible for observations of magnetic field fluctuations in the ionosphere, including a magnetosonic mode predicted by kinetic theory (Espley *et al.*, 2004b). Though a variety of wave properties and modes have been inferred from MAG data, coupling of these data with particle observations or more complete plasma data (e.g. electron oscillations reported by Winningham *et al.* (2006)) would be beneficial to understanding the instabilities responsible for each type of plasma wave at Mars.

Finally, electron data may also be used to provide a global view of the Martian plasma interaction. Figure 8 shows that the average electron flux at 300 eV is highest in the sheath, at low solar zenith angles. Below the MPB the flux drops abruptly, consistent with the electron signatures observed at the MPB in MGS data (see Section 4.4).

### 4.2. Upstream and Foreshock

The upstream and foreshock regions of Mars were visited early in the premapping mission phase, while the MGS orbit periapsis altitude was still high. The typical magnetic field upstream from the shock is 2–4 nT and conforms to the expected Parker spiral configuration of 56° (Crider *et al.*, 2001; Brain *et al.*, 2003). As mentioned above, analysis of oscillations in MAG data confirmed the presence of plasma waves near the proton gyrofrequency (Brain *et al.*, 2002; Mazelle *et al.*, 2004), which are also seen as oscillations in electron data (Mazelle *et al.*, 2004). These waves have been interpreted as standing waves resulting from the interaction of solar wind ions with planetary ions (Mazelle *et al.*, 2004), and as resulting from direct pickup of planetary hydrogen (Russell *et al.*, 1990). MAG data also contained evidence for previously undetected whistler waves in the Martian foreshock (Brain *et al.*, 2002), which have properties at Mars consistent with expectations based on observations at other solar system bodies (see Orlowski and Russell, 1995). Finally, hot diamagnetic cavities upstream of the Martian shock have been reported from MGS data (Figure 9), analogous to hot flow anomalies at Earth believed to result from the interaction of solar wind discontinuities with the bow shock (Øieroset *et al.*, 2001). Upstream phenomena have been reviewed in detail by Mazelle *et al.* (2004); Bertucci *et al.* (2005a).

### 4.3. Boundary Shapes

MGS greatly increased the number of crossings of plasma boundaries, allowing quantitative fits to idealized shapes for the bow shock and MPB and comparison with fits based on previous measurements. Vignes *et al.* (2000) calculated a bow shock shape based on MGS crossings (shown in Figure 1), and Trotignon *et al.* (2006) have calculated a shape combining crossings detected in MGS MAG data and Phobos plasma wave data. These fits are similar to previous fits, summarized in Trotignon *et al.* (2006), though are more accurate due to the greater number of crossings and better solar zenith angle coverage. The Martian bow shock is located at altitudes of ∼2000 km near the subsolar point, and ∼5500 km near the terminator, and appears to be insensitive to solar cycle (Vignes *et al.*, 2000). However, the shape of the bow shock is asymmetric with respect to IMF direction (Dubinin *et al.*, 1998; Vignes *et al.*, 2002), and in general appears to be highly variable. The use of a "best-fit" bow shock shape then is only a first step toward understanding the shape and

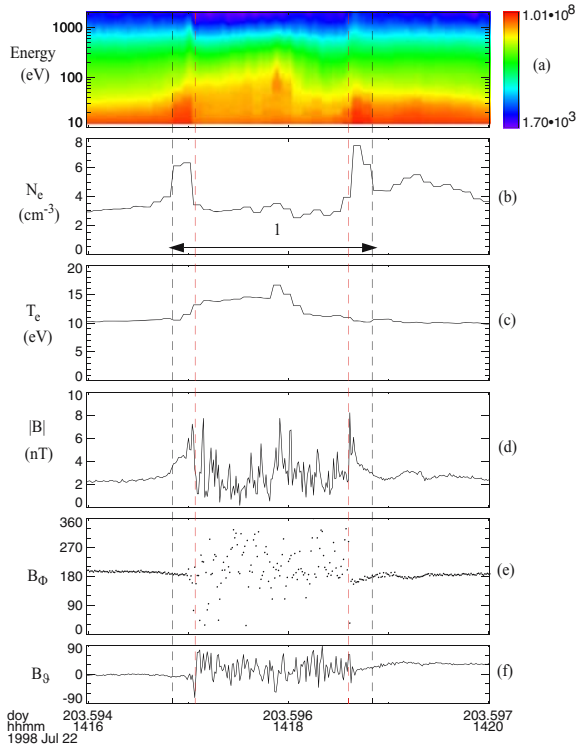


*Figure 9.* Hot diamagnetic cavity upstream of the Martian shock, with regions of high density and magnetic field surrounding a central hot, turbulent plasma with the same density as the undisturbed solar wind. This event is associated with an IMF rotation. From Øieroset *et al.* (2001).

location of the shock. Future studies might account for a number of controlling factors in order to parameterize the shape of the bow shock as a function of location and external conditions. With more than 700 crossings (Trotignon *et al.*, 2006), not including those already returned by MEX, such a study will soon be possible.

MGS increased the number of recorded MPB crossings at Mars from 41 (from Phobos) to nearly 900. The shape has been fit using Phobos data (Trotignon *et al.*, 1996), MGS data (Vignes *et al.*, 2000), a combination of Phobos and MGS data (Trotignon *et al.*, 2006), and MEX data (Dubinin *et al.*, this issue). The four modeled shapes are in rough agreement. A peculiar feature of the Vignes *et al.* (2000) fit (shown in Figure 1) is that the MPB has higher altitudes near the subsolar point than at moderate solar zenith angles. This result is almost certainly not physical and simply results from the assumed shape for the boundary (an ellipsoid offset from the center of Mars), coupled with the lack of coverage by MGS of low solar zenith angles (see Section 2.2 and Figure 2). From the model fits, the MPB is situated at ∼850 km altitudes near the subsolar point, and ∼1500 km near the terminator. Similar to the bow shock, the MPB location is highly variable, and the variability

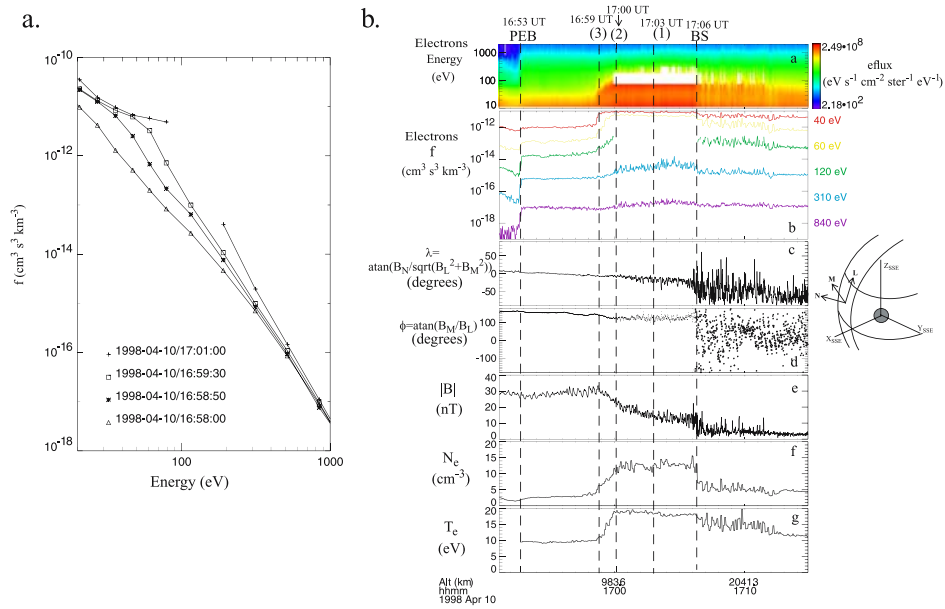


*Figure 10.* Signatures of the MPB in MGS data. (a) Superthermal electron fluxes decrease across the MPB. (b) Changes in electron fluxes, field strength, turbulence, and orientation are observed across the MPB, along with changes in electron density and temperature. Magnetic field is shown in a minimum variance coordinate system. From Øieroset *et al.* (2004).

increases with solar zenith angle. Factors that control the location of the MPB are discussed in Section 5.2.

The PEB observed by MGS is known to be highly variable in its location (discussed further in Section 5.2). Using a combination of premapping and mapping MGS data, the PEB could also be fit to a model shape. Such an effort, incorporating the many thousands of crossings in MGS premapping and mapping observations, should be undertaken in the future.

## 4.4. MPB Signatures and Physics

Previous spacecraft to visit Mars have crossed the MPB, and have referred to it by many names (planetopause, ion composition boundary, mantle boundary, protonopause, magnetopause, etc.). The large number of crossings by MGS has enabled several new insights into the signatures and underlying physics responsible for this boundary. The signatures of the MPB in MGS MAG/ER data (crossing from upstream to downstream) include: an increase in field magnitude, a decrease in field fluctuations, an increase in the field 'draping', and a decrease in superthermal electron fluxes (see Figure 10). These signatures have been used in a number of papers to study the MPB shape (Vignes *et al.*, 2000; Trotignon *et al.*, 2006), its

variability (Crider *et al.*, 2002, 2003; Verigin *et al.*, 2004; Brain *et al.*, 2005a), and its similarity in characteristics and structure to boundaries observed at other planets (Bertucci *et al.*, 2005b). Additionally, MGS data show that the dominant ULF waves differ on either side of the MPB (Bertucci *et al.*, 2004).

Despite the many different names and plasma signatures associated with this boundary, it seems clear that it results from the interaction of the shocked solar wind with planetary heavy ions (see discussion in Nagy *et al.*, 2004). Comparisons of models to data suggest that ionization of the exosphere (via electron impact and charge exchange) play a role in creating the signatures observed by MGS (Crider *et al.*, 2000; Chen *et al.*, 2001). Observation of the same boundary by the Phobos instruments allowed a more complete set of identifying signatures to be constructed, including a change in the ion population from solar wind dominated to planetary dominated (e.g. Breus *et al.*, 1991; Dubinin *et al.*, 1996). Continued measurements and comparison to simulations will help to identify the detailed physics responsible for forming and maintaining the MPB. MEX data are already providing important new information (see other papers in this issue).

A "big picture" question about the MPB is whether this apparently common feature of plasma interactions with atmospheres has an analog at magnetized planets. It has been suggested that the MPB has similarities in structure and behavior to the plasma depletion layer upstream of Earth's magnetopause Øieroset *et al.* (2004). Further, the MPB appears to be the inner boundary for solar wind protons, similar to a magnetopause. Of all bodies in the solar system, the question may best be answered through observations at Mars, which exhibits features of both a Venus-like atmospheric interaction (Cloutier *et al.*, 1999) and an Earth-like magnetospheric interaction near crustal sources (see, for example Krymskii *et al.*, 2000).

The interested reader is referred to reviews by Bertucci *et al.* (2005a); Nagy *et al.* (2004) for further information on the MPB.

### 4.5. Ionosphere

The only *in situ* sampling of the ionosphere prior to MGS was made by the Viking Landers during their descent. The ionosphere is detected by the ER instrument on MGS using electron energy spectra (Mitchell *et al.*, 2000). Below the PEB, where contributions from solar wind-like electrons are relatively weak, ER measures features attributable to photoemission of oxygen. The transition from a regime dominated by solar wind electrons to one dominated by photoelectrons (shown in Figure 11), was seen at altitudes ranging from 180–800 km in the northern hemisphere at high solar zenith angles. Multiple crossings, evident in some orbits, indicate detached ionospheric clouds or surface waves (Mitchell *et al.*, 2001a).

In addition to determination of the ionosphere's upper boundary, there has been some progress in measuring the Martian ionosphere using MGS data. Vignes *et al.* (2004) studied flux ropes identified in the Martian ionosphere at high latitudes in

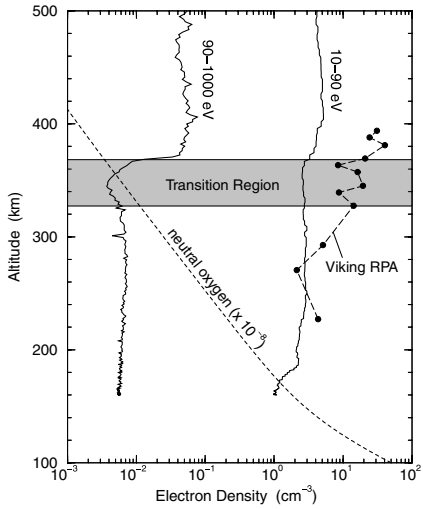


*Figure 11.* Altitude profiles of electron density for two different energy ranges measured by MGS ER. The PEB is located at a sharp transition in 90–1000 eV density. From Mitchell *et al.* (2000).

the northern hemisphere (Cloutier *et al.*, 1999). This preliminary study suggests that flux ropes are observed more often at Venus than Mars (where the ionosphere is often magnetized), and never near crustal fields in the southern hemisphere. The orientation of the draped IMF in the ionosphere, discussed in Section 4.1, has been quantified (Crider *et al.*, 2001). And several studies have analyzed ionospheric profiles measured using radio science, including influences from crustal fields and solar X-ray flux (Krymskii *et al.*, 2002a, 2004, 2002b; Ness *et al.*, 2000; Withers *et al.*, 2005; Mendillo *et al.*, 2003, 2006). In the future, photoelectron fluxes in MGS data might be studied as a function of solar zenith angle and external conditions to learn more about the distribution of ionospheric electrons.

### 4.6. Wake

The wake and tail are particularly important for studies of present day atmospheric escape, since much of the escaping ion flux passes through these regions. MGS lacks ion measurements, and studies of the properties of these regions have necessarily focused on nightside magnetic field structure and superthermal electron distributions (each of which may indirectly provide clues about escaping particles and processes). The central wake and tail was also explored by Phobos, and its thickness and field orientation were used as support for both intrinsic and induced Martian obstacles to the solar wind (Riedler *et al.*, 1989; Russell *et al.*, 1995; Axford, 1991; Möhlmann *et al.*, 1991; Dubinin *et al.*, 1994). Comparison of MGS premapping MPB crossings to a model for the boundary shape by Verigin *et al.* (2004) suggests

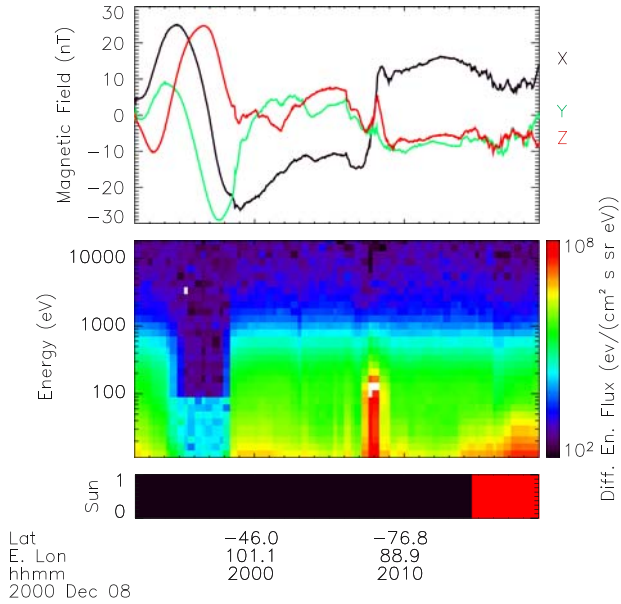


*Figure 12*. Nightside current sheet crossing by MGS. The magnetic field in MSO coordinates (top) has a sharp reversal near 20:08, accompanied by an increase in 10–200 eV electron energy fluxes (middle) Crustal fields are evident at the beginning of the time period. From Halekas *et al*. (2006).

that crustal magnetic fields act to make the tail boundary (the nightside extension of the MPB) thicker by up to 1000 km, so that both intrinsic and induced fields influence the tail structure. MGS mapping data revealed a magnetic flux asymmetry between the two lobes of the induced magnetotail (Ferguson *et al*., 2005). More detailed study of nightside current sheet crossings (inferred from field reversals) shows that the thin current sheets measured at the 400 km mapping altitude of MGS (shown in Figure 12) have locations and variability consistent with reconnection of the draped IMF to crustal magnetic fields (Halekas *et al*., 2006). And Mitchell *et al*. (2001a) showed that electron fluxes at energies less than ∼400 eV are lower in the tail.

Measurements made by MEX in the past two years prompted re-examination of the MGS tail measurements for evidence of particle acceleration. First, UV auroral emission detected by MEX was reported by Bertaux *et al*. (2005) in a region of radial nightside crustal magnetic field. MGS observations during this time show that this observation occurred during the passage of a SEP event through the Martian system, before the arrival of the CME shock (Brain *et al*., 2005b), suggesting a possible link between auroral emission at Mars and SEP events, as has been

suggested for Venus (Phillips *et al.*, 1986). Secondly, Lundin *et al.* (2005) reported nightside ion and electron spectra peaked in energy, indicative of a field-aligned auroral-like acceleration process. Examination of MGS mapping data at much lower altitude revealed thousands of auroral-like peaked electron energy spectra (Brain *et al.*, 2005b), and showed that these spectra occurred unambiguously above regions of radial crustal magnetic field lines, on the edges of closed field regions. The MGS data also revealed that in some locations the observations of auroral-like electron distributions is influenced by IMF direction, Martian season, and (weakly) by solar wind pressure. Each of these dependencies indicates an external influence on the conditions required for observation of accelerated electrons. The upward-accelerated ions seen by Mars Express show that atmospheric escape may occur out of cusps of crustal magnetic field on the Martian night side (Lundin *et al.*, 2005). Further study of particle acceleration signatures, in tandem with MEX UV and particle observations, should prove useful in uncovering how the particles are accelerated and their effect on the Martian atmosphere.

## 5. Variability

The preceding sections of this review have focused in large part on MGS contributions toward describing the steady-state Martian solar wind interaction. However, the particles and fields environment is highly variable. MGS mapping data are particularly useful for exploring variability in the Martian system, since they have been collected in one small region of this interaction over a period now in excess of six years. MGS data have shown how the Sun and solar wind influence plasma boundaries, magnetic fields, and field topology near Mars, and that unexplained asymmetries exist in the data. MGS results on variability are discussed below.

### 5.1. Proxies

There is no upstream solar wind monitor at Mars, and no monitor of solar EUV. Therefore, proxy information derived from MGS and Earth-based observations must be employed in order study external influences on the *in situ* MGS measurements. To date, proxies for solar EUV flux, upstream solar wind pressure, and the clock angle of the IMF have been constructed. Figure 13 shows a timeseries for each of these proxies during the MGS mapping orbit. The proxy for the solar EUV flux at Mars has been inferred from the F10.7 radio flux measured at Earth, extrapolated from 1 AU to the heliocentric distance of Mars, and time-shifted to account for the difference in solar longitude of Mars and Earth (Mitchell *et al.*, 2000).

Magnetic pressure on the day side, far from crustal fields, is assumed to be proportional to upstream solar wind dynamic pressure in a proxy developed by Crider *et al.* (2003). This method compares favorably with extrapolation of Earth-based

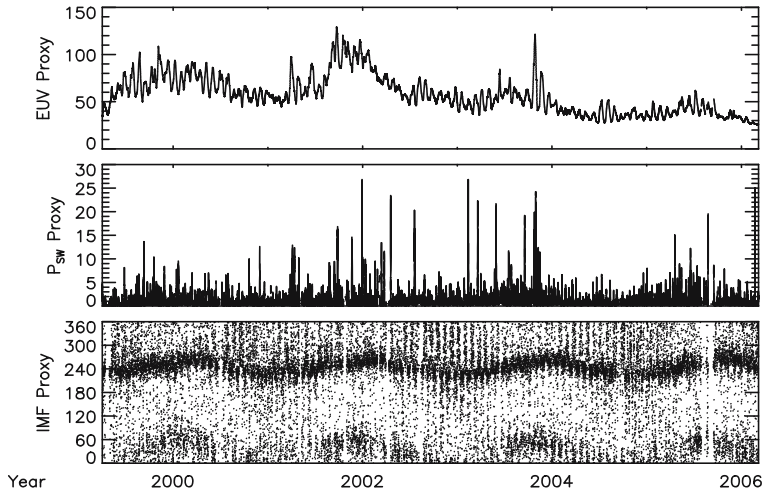


*Figure 13.* Three proxy datasets for Mars: EUV flux in solar flux units (top); solar wind pressure in units of nPa (middle); and IMF draping direction in degrees (bottom).

measurements to Mars' orbital distance. Pressure values are computed on an orbit-by-orbit basis, and assume that sudden changes in pressure do not occur during each two-hour orbit period. Further, the MPB is pushed below the mapping altitude of MGS on ∼20% of the mapping orbits, so that magnetic pressure in the sheath, rather than the pileup region, is used to calculate the proxy (Brain *et al.*, 2005a). In the sheath, however, the thermal plasma pressure may constitute a larger fraction of the total pressure, so that use of magnetic pressure alone provides an underestimate of the upstream solar wind pressure. For these reasons pressure proxy information is best-used in statistical studies that seek to separate high pressure time periods from low pressure time periods. In addition to the MGS-based pressure proxy, Vennerstrom *et al.* (2003) have extrapolated ACE data to the heliocentric distance of Mars during time periods when Mars and Earth were magnetically aligned.

The orientation of the IMF upstream from Mars has been estimated in three different ways. For pre-mapping data, (Crider *et al.*, 2004) determined the IMF draping direction from field vectors recorded immediately downstream from the bow shock, where field amplitudes are large enough that the determination is not overly sensitive to spacecraft-generated magnetic fields. For mapping data, Brain *et al.* (2006) used the configuration of the draped IMF on the dayside, far from crustal fields, as indicative of the clock angle of the upstream IMF. Like the proxy for solar wind pressure, both these methods calculate a proxy on an orbit-by-orbit basis, and assume that external conditions do not change during each orbit. Vennerstrom *et al.* (2003) showed that, for time periods when Earth and Mars are magnetically aligned, ACE data provide an adequate estimate of the IMF orientation on timescales associated with solar wind sector changes.

TABLE I

Drivers affecting variability in the location of plasma boundaries at Mars, and references to analyses of MGS data.

| | Bow shock | MPB | PEB |
|---|---|---|---|
| Solar wind pressure | ? | Yes[a] | Yes[b] |
| IMF direction | Yes[c] | Yes[d] | ? |
| EUV | ? | ? | Yes[e] |
| Martian season | ? | Yes/?[d] | ? |
| Crustal fields | No/?[c] | Yes[a] | Yes[b] |

[a]Crider *et al*. (2003).

[b]Mitchell *et al*. (2001b).

[c]Vignes *et al*. (2002).

[d]Brain *et al*. (2005a).

[e]Mitchell *et al*. (2000).

[f]Crider *et al*. (2002).

## 5.2. Boundaries

The response of the location of plasma boundaries near Mars to different influences has been well-studied. Table I shows whether the bow shock, MPB, and PEB have been demonstrated to vary in response to five drivers using MGS data. High solar wind pressure compresses both the MPB and the PEB, and likely similarly affects the bow shock (Crider *et al*., 2003; Mitchell *et al*., 2001b). The IMF direction controls the direction of the solar wind convection electric field ($\mathbf{E}_{SW} = -\mathbf{v}_{SW} \times \mathbf{B}$), which in turn affects the motion of charged particles in the planetary interaction region. The bow shock and MPB have both been shown to have asymmetric shapes (or, less likely, to change size) determined by the IMF orientation (Vignes *et al*., 2002; Brain *et al*., 2005b). Mass loading of the flow by planetary heavy ions is thought to influence the global interaction at Mars similar to comets, particularly near the MPB. It has not yet been demonstrated whether mass loading is directly responsible for the observed variability through creation of a hemispherically asymmetric obstacle to the flow, or whether simple particle motion controls the observed asymmetries. Solar EUV flux, initially shown to have little influence on the PEB location (Mitchell *et al*., 2000), has more recently been demonstrated to raise the altitude of the PEB during observations made when the EUV flux is high (Mitchell *et al*., 2001b). Seasonal effects have been observed in the location of the MPB (Brain *et al*., 2005b), but this influence is thought to be caused indirectly by crustal fields, which are strongest at southern mid-latitudes and therefore approach closer to the subsolar point during southern summer, raising the altitude of the MPB. Finally, the effects of crustal fields have been reported for the location of the PEB

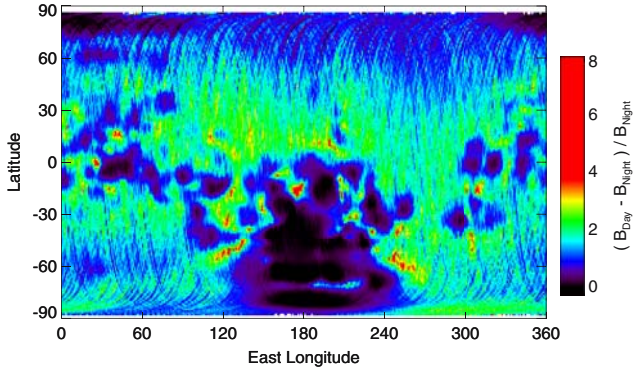


*Figure 14.* Geographic map of compression in the magnetic field magnitude, expressed as $\Delta B/B_{\text{night}}$, where $\Delta B = B_{\text{day}} - B_{\text{night}}$.

and MPB (Mitchell *et al.*, 2001a; Crider *et al.*, 2002), but have not been definitively measured for the more distant bow shock (Vignes *et al.*, 2002).

### 5.3. Field and Topology

Variability has been detected in MGS MAG measurements of field amplitude and orientation throughout the Martian system. One example is the day-night variability shown in Figure 14. The figure shows the increase in field magnitude on the day side in many geographic locations, relative to the field magnitude at each location on the night side. On average, at mid-latitudes the dayside field is a factor of two or more higher than on the night side, with large increases in certain regions near crustal sources. This excess field on the dayside likely has two sources: the draped IMF and current-generated magnetic fields. One unexplained feature of this map is a $\sim$(20%) reduction in average field strengths on the day side relative to the night side in some regions of strong horizontal crustal magnetic field. Other variability in magnetic field demonstrated using MGS data includes the influence of upstream pressure and IMF direction on the night side (Ferguson *et al.*, 2005; Brain *et al.*, 2006). These analyses show that external influences have not been entirely removed from the data also used to construct models for the crustal magnetic fields (Purucker *et al.*, 2000; Arkani-Hamed, 2001; Cain *et al.*, 2003; Langlais *et al.*, 2004).

Field topology, determined from ER and MAG measurements exhibits variability on both the night side and day side with IMF direction and upstream pressure. Figure 15 shows geographic probability maps of the likelihood of observing one-sided loss cone distributions in ER pitch angle data for two sets of MGS orbits. For orbits where the IMF on the Martian day side is roughly westward, there is a low probability of observing distributions associated with open field lines in the region centered near (210°E, 45°S). For eastward IMF, however, open field lines are often

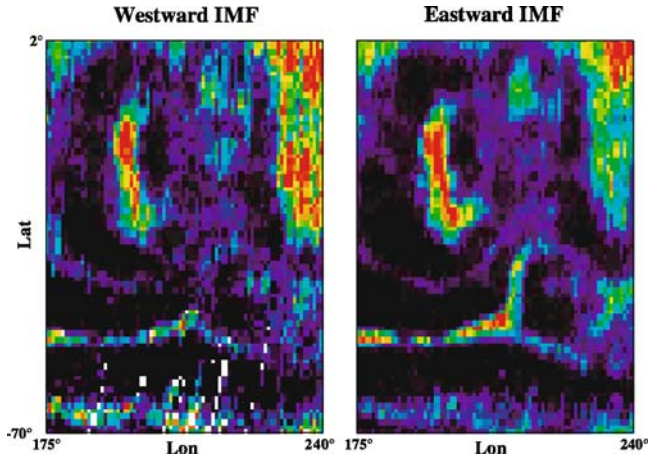


*Figure 15*. Geographic probability maps of one-sided loss cone distributions, analogous to Figure 7b, separated according to IMF direction.

observed, indicating that IMF direction in part determines whether a crustal field cusp at 400 km is open or closed. Other differences between the two maps are evident in the figure, and may be associated with topological changes governed by the IMF orientation. This change in topology could be achieved by magnetic reconnection, or by large scale motion of closed and open field regions – both governed by IMF direction. Variability in topology has also been measured for upstream pressure variations (Brain *et al*., 2004).

### 5.4. Asymmetries

A number of unusual field asymmetries have been discovered in MAG/ER data, and their origin has not been fully resolved. First, Krymskii *et al*. (2002a) discovered that the total magnetic flux calculated from a map of the median nightside magnetic field (Connerney *et al*., 2001) is non-zero, with significant additional flux toward the planet. The map was constructed from observations made over a long time period, so that the different directions of the IMF should have largely averaged out of the map. This observation of non-zero flux may simply result from the fact that the magnetic field map used in the calculation was not made over a closed surface; instead Mars rotated underneath the spacecraft situated at fixed local time as statistics were accumulated in each bin. Therefore, a negative net flux at the 2am orbit may be compensated by a net positive flux at other local times. Ferguson *et al*. (2005) also observed an asymmetry in the sunward component of the nightside magnetic field, after a spherical harmonic crustal field model was subtracted (see Figure 16). Further, the asymmetry between the number of observations with B toward the Sun/planet vs. away grew with upstream solar wind pressure. Brain *et al*.

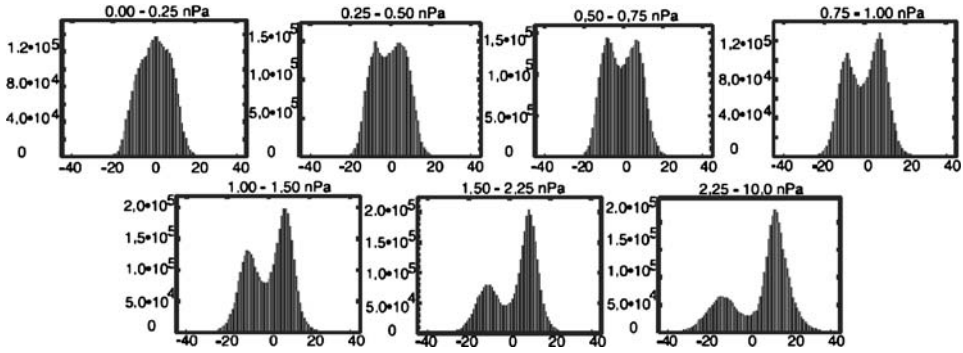


*Figure 16*. Histograms of the sunward component of magnetic field on the Martian night side, after the Cain *et al*. (2003) crustal magnetic field model has been subtracted, separated according to upstream pressure. From Ferguson *et al*. (2005).

(2006) showed an asymmetry in the nightside radial field component controlled by IMF direction. This asymmetry might be explained by an asymmetrically shaped MPB and tail, however there is a peculiar long-wavelength dependence of the asymmetry on planetary longitude which remains unexplained. Finally, Brain *et al*. (2006) showed an asymmetry in the draping directions of the magnetic field on the day side in the northern hemisphere, where draping directions cluster in a direction pointed toward the subsolar point when Mars is in one sector of the solar wind, but not the other. This asymmetry might be explained by an asymmetry in "weather-vaning" of the draped field in the ionosphere for one IMF direction, coupled with the asymmetrically shaped MPB mentioned above. "Weathervaning" refers to the antisolar draping of the low-altitude portion of magnetic field lines as they are embedded in the ionosphere, and was observed extensively at Venus (Law and Cloutier, 1995) and reported at Mars (Cloutier *et al*., 1999).

### 5.5. SEP Effects

A more extreme source of variability has been observed at Mars in the form of Solar Energetic Particle (SEP) events. SEP events are associated with Coronal Mass Expansions (CMEs) from the Sun, and charged particles can be accelerated to energies of hundreds of MeV near the Sun or at the shock front of the CME as it expands and propagates into the solar system. The influence of SEP events, many of which have also been observed at Earth, has been detected in MAG/ER data and related to effects measured by other spacecraft instruments in the upper atmosphere. A particularly large event occurred at Earth on 28 October 2003, and is referred to as the Halloween 2003 event. During this event, MGS observed compression of the Martian system and an increase of field strengths on the day side (Crider *et al*., 2005). Solar wind access to low altitudes (determined from electron

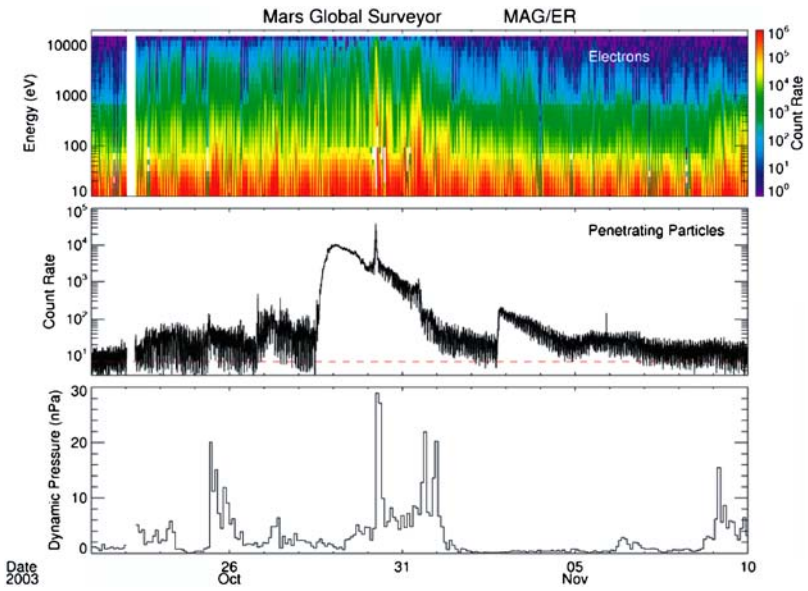


*Figure 17.* The Halloween 2003 solar events at Mars. (Top) Flux of energetic (10–20 keV) electrons measured by ER, after subtraction of SEPs and GCRs. (Middle) Count rate of SEP and GCR particles penetrating the ER instrument. (Bottom) Solar wind pressure proxy. (Figure courtesy of D. Mitchell).

measurements) increased (Crider *et al*., 2005), and waves near the gyrofrequency of pickup hydrogen and oxygen were observed on the typically quiet night side (Espley *et al*., 2005). Each of these observations suggests that atmospheric escape rates are elevated during solar storms, which may be more reminiscent of conditions early in Martian history. Recently, MARSIS radar observations have been shown to contain evidence for additional ionization layers in the atmosphere during the times of SEP events (Morgan *et al*., 2006).

Figure 17 shows a timeseries of background countrates from the ER during a large SEP event at Mars, and the solar wind pressure proxy during this time period. The three highest energy channels of the ER instrument (10–20 keV) typically measure background, which is dominated at quiet times by the Galactic Cosmic Ray (GCR) flux. However, the ER is sensitive to solar energetic protons with energies of 10's MeV, which directly penetrate the instrument housing and strike the instrument anode to be recorded as counts. The countrate of penetrating particles (SEPs and GCRs) is independent of the ER energy channel, since these particles do not pass through the instrument optics and are therefore unaffected by the energy to which the instrument is tuned. For large penetrating particle fluxes, then, the three highest energy channels have nearly equal countrates when the signal is dominated by penetrating particles, and unequal countrates when there are significant numbers of 10–20 keV electrons present. The event is apparent in ER data as a rise in

background countrate in all energy channels equally on 28–29 October, followed by a spike in the ER countrate and associated increase in solar wind pressure on 30 October, followed by a steady decline during which there are large temporal variations in the ER backgrounds as well as a consistently lower countrates in the highest energy channel. These three phases are interpreted as an initial period where SEPS accelerated in front of the CME shock encounter the Martian system, followed by the passage of the shock by Mars, and a timeperiod where both SEPs and energetic electrons are measured by ER. This event is only one of many tens of examples of SEP events detected by ER at Mars during the mapping phase of the mission, and we estimate that ∼4% of MGS observations occur during SEP events.

## 6. Summary

The Martian plasma interaction has similarities to the atmospheric interaction at Venus and comets, and to a magnetospheric interaction at Earth or on small scales at the Moon. The main features of the Martian solar wind interaction region are well-known, including a bow shock, magnetosheath, MPB (or alternatively named boundary), MPR, ionosphere, wake, tail, and plasma sheet. In addition, crustal magnetic fields are an important part of the interaction. The solar wind interaction has bearing on the problems of atmospheric escape and climate evolution at Mars, the structure and variability of the upper atmosphere, and on fundamental plasma processes such as reconnection and particle acceleration. A number of spacecraft have made relevant measurements at Mars, dating back more than forty years.

MGS carries a vector magnetic field instrument and an electrostatic analyzer, dedicated to study of the plasma environment and intrinsic magnetic field at Mars. Magnetometers and electron measurements had both been made at Mars before, but the unprecedented orbit of MGS enabled many new discoveries. The spacecraft went much lower than any previous spacecraft carrying plasma instruments, covered the global interaction region better than any previous spacecraft during its elliptical aerobraking period, and has made mapping observations from ∼400 km and fixed local time for more than six years. This orbit allowed discovery of crustal sources, characterization of different regions of the interaction, and determination of variability in response to many different drivers and on many timescales.

Crustal fields are sufficiently strong that they extend upward into the plasma interaction and modify it. Because they contribute magnetic pressure that helps the ionosphere divert the solar wind, they perturb the locations of boundaries, and may fundamentally change their nature. Crustal fields also enable new magnetic topologies, including closed field lines that shield portions of the atmosphere from the solar wind, and open field lines that allow access of the solar wind to the lower ionosphere (and particle escape).

MGS has made new discoveries and contributions in each region of the solar wind interaction. The entire system has been visualized using MAG/ER data in various forms. Hot diamagnetic cavities have been observed upstream and whistler waves have been detected in the foreshock. The shape of the bow shock and MPB have been determined with greater accuracy. New defining features of the MPB have been defined and compared to similar boundaries at other planets, and the role of ionization processes in creating the boundary has been explored. Flux ropes have been observed in the ionosphere, and the upper boundary to the ionosphere has been characterized as a function of location and external drivers. Evidence for electron acceleration in cusps of crustal magnetic field has been reported, and low-altitude current sheets have been reported, possibly resulting from reconnection of the draped IMF with crustal fields.

Variability has been observed throughout the system. The bow shock, MPB, and PEB have all been observed to respond to external drivers, including solar wind pressure, IMF direction, EUV fluxes, crustal fields, and Mars' orientation with respect to the Sun and solar wind. MGS data have proved capable of supplying proxy information about the upstream solar wind pressure and IMF orientation. This proxy information is useful for organizing both MGS and MEX observations. The bow shock and MPB are both asymmetrically shaped, with the asymmetry apparently controlled by the IMF direction. Magnetic field magnitude, orientation, and topology all respond to conditions in the upstream solar wind. Asymmetries have been observed in magnetic field measurements which have not yet been completely explained. SEP events noticeably disturb the Martian system, compressing the interaction region after the arrival of a CME shock, increasing atmospheric escape fluxes, and depositing energy in the upper atmosphere.

### 6.1. Looking Forward

Though the many contributions from MGS have been summarized in this review, it is likely that many more will follow. Three different avenues of research should bring new results from MGS. First, the existing MGS premapping and mapping data have not yet been fully mined for the information they carry. Promising areas include further analysis of the ER angular electron distributions, investigation of high time resolution vector magnetic field data for waves and discontinuities, and investigation of the detailed physical processes (such as reconnection and particle acceleration) likely evident in mapping orbit data.

Second, MAG/ER continues to make measurements from the MGS mapping orbit, and may do so for several more years. New data would undoubtedly promote new discoveries. Additionally, a few more years of observations would enable investigation of the dataset over an entire solar cycle at Mars, and reduce uncertainties in statistical analyses (for example, investigation of mapping orbits recorded during periods of high solar wind pressure, only).

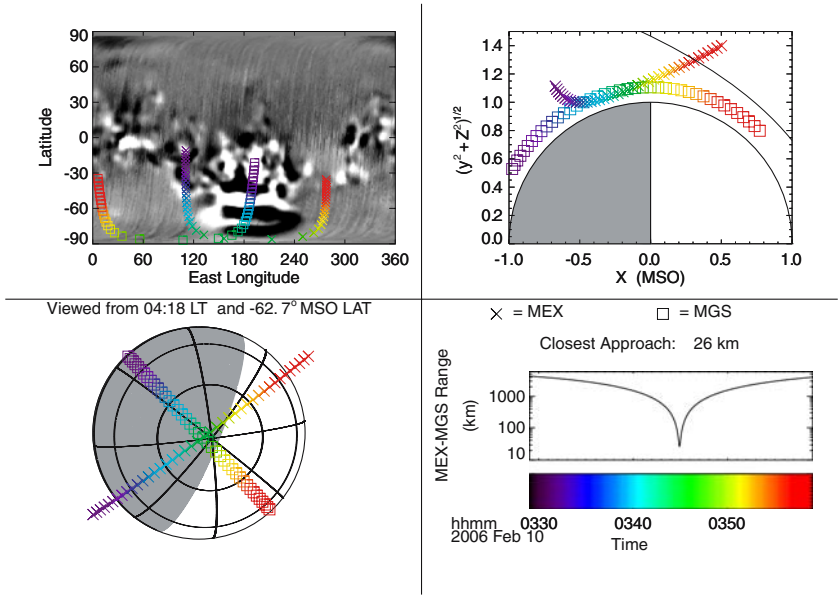


*Figure 18.* Orbit geometry for MGS and MEX during a close spacecraft pass. Trajectories are colored according to time (bottom right), with × denoting MEX position and square denoting MGS position. Trajectories are shown in rectangular planetary coordinates (top left), MSO cylindrical coordinates (top right), and in satellite projection (bottom left).

Finally, simultaneous measurements by other spacecraft may enhance the scientific return of MAG/ER, and vice versa. Since early 2004, MGS and MEX have been making *in situ* measurements of the plasma environment that are complementary (in terms of both instrument and orbit). Each of MGS and MEX data in tandem provides an opportunity to mitigate the shortcomings of each dataset, and increase our overall understanding of the Martian solar wind interaction and atmospheric escape. Close passes of spacecraft (conjunctions) are one particularly powerful means of increasing the utility of measurements, as evidenced by the Cluster mission at Earth. At Mars, conjunctions might be used to obtain more complete simultaneous and/or co-located plasma measurements, which can be used to study a variety of phenomena, including measurements of auroral-like particle acceleration near crustal fields and the three-dimensional motion and shape of plasma boundaries.

Approximately forty conjunctions (instances with instantaneous spacecraft separation smaller than 400 km) of MGS and MEX have already been identified between January 2004 and February 2006. The closest pass was 27 km, near the South Pole (Figure 18). Conjunctions occur both at mid-latitudes (when the surface-projected orbit tracks of the two spacecraft nearly overlap), and at the poles. These conjunctions will be explored further in the coming months, including intercomparison of MGS and MEX electron data, the addition of MGS magnetic field and MES

ion data, and the inclusion of solar wind proxy information to establish context. Other configurations of MGS and MEX may also prove useful, including times when they are on the same flux tube (for spatial evolution of particle distributions), times when they pass through the same region of space separated by a delay (for time evolution of plasma populations in certain regions), and times when they are on opposite sides of plasma boundaries (to determine boundary shapes and motion).

Comparison of MGS observations simultaneous with those of other spacecraft is already proving quite useful in understanding the system. Measurements from the Mars Express instruments ASPERA-3 (e.g. Fedorov *et al*., 2006) and MARSIS (e.g. Morgan *et al*., 2006) have been compared with MGS-derived solar wind proxies and observations. Continued study of simultaneous MGS-MEX observations will provide leverage needed to better understand the interaction of the solar wind with the Martian atmosphere.

## Acknowledgement

D. Brain acknowledges the useful discussions and input of D. Mitchell, J. Halekas, D. Crider, and J. Luhmann in preparing this manuscript.

## References

Acuña, M. H., Connerney, J. E. P., Wasilewski, P., Lin, R., Anderson, K., Carlson, C. W., *et al*.: 1992, *J. Geophys. Res.* **97**, 7799.

Acuña, M. H., Connerney, J. E. P., Wasilewski, P., Lin, R., Anderson, K., Carlson, C. W., *et al*.: 1998, *Science* **279**, 1676.

Acuña, M. H., Connerney, J. E. P., Ness, N., Lin, R., Mitchell, D., Carlson, C. W., *et al*.: 1999, *Science* **284**, 790.

Acuña, M. H., Connerney, J. E. P., Ness, N., Lin, R., Mitchell, D., Carlson, C. W., *et al*.: 2001, *J. Geophys. Res.* **106**(E10), 23,403.

Albee, A. L., Arvidson, R.E., Palluconi, F., and Thorpe, T.: 2001, *J. Geophys. Res.* **106**(E10), 23,291.

Arkani-Hamed, J.: 2001, *J. Geophys. Res.* **106**(E10), 23,197.

Axford, W. I.: 1991, *Planet Space Sci.* **39**(7), 167.

Barabash, S., and Lundin, R.: 2006, *Icarus* **182**(2), doi: 10.1016/j.icarus.2006.02.015.

Bertaux, J. L., Leblanc, F., Witasse, O., Quemerais, E., Lilensten, J., Stern, S. A., *et al*.: 2005, *Nature* **435**, doi: 10.1038/nature03603.

Bertucci, C., Mazelle, C., Crider, D. H., Mitchell, D. L., Sauer, K., Acuña, M. H., *et al*.: 2004, *Adv. Space Res.* **33**, 1938, doi: 10.1016/j.asr.2003.04.054.

Bertucci, C., Mazelle, C., and Acuña, M. H.: 2005a, *J. Atm. Terr. Phys.* **67**(17–18), 1797, doi: 10.1016/j.jastp.2005.04.007.

Bertucci, C., Mazelle, C., Acuña, M. H., Russell, C. T., and Slavin, J. A.: 2005b, *J. Geophys. Res.* **110**, A01209, doi: 10.1029/2004JA010592.

Bogdanov, A. V., and Vaisberg, O. L.: 1975, *J. Geophys. Res.* **80**, 487.

Brain, D. A.: 2002, PhD thesis, University of Colorado.

Brain, D. A., and Jakosky, B. M.: 1998, *J. Geophys. Res.* **103**(E10), 22,689.

Brain, D. A., Bagenal, F., Acuña, M. H., Connerney, J. E. P., Crider, D. H., Mazelle, C., *et al*.: 2002, *J. Geophys. Res.* **107**(A6), 1076, doi: 10.1029/2000JA000416.

Brain, D. A., Bagenal, F., Acuña, M. H., and Connerney, J. E. P.: 2003, *J. Geophys. Res.* **108**(A12), 1424, doi: 10.1029/2002JA009482.

Brain, D. A., Mitchell, D. L., Lillis, R., and Lin, R.: 2004, AGU Fall Meeting Abstracts pp SA13A–1119 (abstract).

Brain, D. A., Halekas, J. S., Lillis, R. J., Mitchell, D. L., Lin, R. P., and Crider, D. H.: 2005a, *Geophys. Res. Lett.* **32**(18), L18203, doi: 10.1029/2005GL023126.

Brain, D. A., Halekas, J. S., Peticolas, L. M., Lin, R. P., Luhmann, J. G., Mitchell, D. L., *et al*.: 2005b, *Geophys. Res. Lett.* **33**(1), L01201, doi: 10.1029/2005GL024782.

Brain, D. A., Mitchell, D. L., and Halekas, J. S.: 2006, *Icarus* **182**(2), 464, doi: 10.1016/j.icarus.2005.09.023.

Breus, T. K., Krymskii, A. M., Lundin, R., Dubinin, E. M., Luhmann, J., Yeroshenko, Y., *et al*.: 1991, *J. Geophys. Res.* **96**(A7), 11,165.

Cain, J. C., Ferguson, B. B., and Mozzoni, D.: 2003, *J. Geophys. Res.* **108**(E2), 5008, doi: 10.1029/2000JE001487.

Carlsson, E., Fedorov, A., Barabash, S., Budnik, E., Grigoriev, A., Gunell, H., *et al*.: 2006, *Icarus* **182**(2), 320, doi: 10.1016/j.icarus.2005.09.020.

Chen, Y., Cloutier, P. A., Crider, D. H., Mazelle, C., and Rème, H.: 2001, *J. Geophys. Res.* **106**(A12), 29,387.

Cloutier, P. A., Law, C. C., Crider, D. H., Walker, P. W., Chen, Y., Acuña, M. H., *et al*.: 1999, *Geophys. Res. Lett.* **26**(17), 2685.

Connerney, J. E. P., Acuña, M. H., Wasilewski, P. J., Kletetschka, G., Ness, N. F., Rème, H., *et al*.: 2001, *Geophys. Res. Lett.* **28**(21), 4015.

Connerney, J. E. P., Acuña, M. H., Ness, N. F., Kletetschka, G., Mitchell, D. L., Lin, R. P., *et al*.: 2005, *Proc. Nat. Acad. Sci.* **102**(42), 14,970, doi: 10.1073/pnas.0507469102.

Crider, D.: 2004, *Adv. Space Res.* **33**, 152, doi: 10.1016/j.asr.2003.04.013.

Crider, D., Cloutier, P., Law, C., Walker, P., Chen, Y., Acuña, M., *et al*.: 2000, *Geophys. Res. Lett.* **27**(1), 45.

Crider, D., Acuña, M., Connerney, J., Mitchell, D., Lin, R., Cloutier, P., *et al*.: 2001, *Adv. Space Res.* **27**(11), 1831.

Crider, D., Brain, D. A., Acuña, M., Vignes, D., Mazelle, C., and Bertucci, C.: 2004, *Space Sci. Rev.* **111**, 203.

Crider, D., Espley, J., Brain, D. A., Mitchell, J. E. P., Connerney, D. L., and Acuña, M.: 2005, *J. Geophys. Res.* **110**(A9), A09S21, doi: 10.1029/2004JA010881.

Crider, D. H., Acuña, M. H., Connerney, J. E. P., Vignes, D., Ness, N. F., Krymskii, A. M., *et al*.: 2002, *Geophys. Res. Lett.* **29**, 11.

Crider, D. H., Vignes, D., Krymskii, A. M., Breus, T. K., Ness, N. F., *et al*.: 2003, *J. Geophys. Res.* **108**(A12), 1461, doi: 10.1029/2003JA009875.

Dolginov, S. S., Yeroshenko, Y. G., and Zhuzgov, L. N.: 1976, *J. Geophys. Res.* **81**, 3353.

Dubinin, E., Fraenz, M., Woch, J., Roussos, E., Barabash, S., Lundin, R., *et al*.: *Space Sci.Rev.*, this issue, doi: 10.1007/s11214-006-9039-4.

Dubinin, E., Lundin, R., Norberg, O., and Pissarenko, N.: 1993, *J. Geophys. Res.* **98**(A11), 3991.

Dubinin, E., Lundin, R., and Schwingenschuh, K.: 1994, *J. Geophys. Res.* **99**(A11), 21,233.

Dubinin, E., Sauer, K., Lundin, R., Norberg, O., Trotignon, J. G., Schwingenschuh, K., *et al*.: 1996, *J. Geophys. Res.* **99**(A12), 27,061.

Dubinin, E., Sauer, K., Delva, M., and Tanaka, T.: 1998, *Earth Planets Space* **50**, 873.

Ergun, R. E., Andersson, L., Peterson, W. K., Brain, D., Delory, G. T., Mitchell, D. L., *et al*.: 2006, *Geophys. Res. Lett.* **33**, L14103, doi: 10.1029/2006GL025785.

Espley, J., Cloutier, P. A., Brain, D. A., Crider, D. H., and Acuña, M. H.: 2004a, *J. Geophys. Res.* **109**, A07213, doi: 10.1029/2003JA010193.

Espley, J., Delory, G. T., and Cloutier, P. A.: 2004b, *J. Geophys. Res.* **111**, E06S22, doi: 10.1029/2005JE002587.

Espley, J., Cloutier, P. A., Crider, D. H., Brain, D. A., and Acuña, M. H.: 2005, *J. Geophys. Res.* **110**, A09S33, doi: 10.1029/2004JA010935.

Fedorov, A., Budnik, E., Sauvaud, J. A., Mazelle, C., Barabash, S., Lundin, R., *et al.*: 2006, *Icarus* **182**(2), 329, doi: 10.1016/j.icarus.2005.09.021.

Ferguson, B., Cain, J. C., Crider, D. H., Brain, D. A., and Harnett, E.: 2005, *Geophys. Res. Lett.* **32**(16), L16105, doi: 10.1029/2004GL021964.

Fillingim, M. O., Peticolas, L. M., Lillis, R. J., Brain, D. A., Halekas, J. S., Mitchell, D. L., *et al.*: 2006, European Geophysical Union 2006 meeting, pp EGU06–A–09,238 (abstract).

Fraenz, M., Dubinin, E., Roussos, E., Woch, J., Winningham, J. D., Frahm, R., *et al.*: *Space Sci. Rev.*, this issue, doi: 10.1007/s11214-006-9115-9.

Futaana, Y., Barabash, S., Grigoriev, A., Holmström, M., Kallio, E., Brandt, P. C., *et al.*: 2006, *Icarus* **182**(2), 424, doi: 10.1016/j.icarus.2005.09.019.

Gurnett, D. A., Kirchner, D. L., Huff, R. L., Morgan, D. D., Persoon, A. M., Averkamp, T. F., *et al.*: 2005, *Science* **310**(5756), doi: 10.1126/science.1121868.

Halekas, J. S., Brain, D. A., Lillis, R. J., Fillingim, M. O., Mitchell, D. L., and Lin, R. P.: 2006, *Geophys. Res. Lett.* **33**, L13101, doi: 10.1029/2006GL026229.

Hanson, W. B., Santani, S., and Zuccaro, D. R.: 1977, *J. Geophys. Res.* **82**(28), 4351.

Harnett, E. M. and Winglee, R. M.: 2003, *Geophys. Res. Lett.* **30**(20), 2074, doi: 10.1029/2003GL017852.

Harnett, E. M., and Winglee, R. M.: 2005, *J. Geophys. Res.* **110**(A7), A07226, doi: 10.1029/2003JA010315.

Hinson, D. P., Simpson, R. A., Twicken, J. D., Tyler, G. L., Flasar, F. M.: 1999, *J. Geophys. Res.* **104**(E11), 26,297.

Jakosky B. M., Phillips R. J. (2001) Mars volatile and climate history. *Nature* **412**(6843), 237.

Krymskii, A. M., Breus, T. K., Ness, N. F., and Acuña, M. H.: 2000, *Space Sci. Rev.* **92**(A9), 535.

Krymskii, A. M., Breus, T. K., Ness, N. F., Acuña, M. H., Connerney, J. E. P., Crider, D. H., *et al.*: 2002a, *J. Geophys. Res.* **107**(A9), 1245, doi: 10.1029/2001JA000239.

Krymskii, A. M., Breus, T. K., Ness, N. F., Hinson, D. P., and Bojkov, D. I.: 2002b, *J. Geophys. Res.* **108**(A12), 1431, doi: 10.1029/2002JA009662.

Krymskii, A. M., Ness, N. F., Crider, D. H., Breus, T. K., Acuna, M. H., and Hinson, D. P.: 2004, *J. Geophys. Res.* **109**, A11306, doi: 10.1029/2004JA010420.

Langlais, B., Purucker, M. E., and Mandea, M.: 2004, *J. Geophys. Res.* **109**(E18), 2008, doi: 10.1029/2003JE002048.

Law, C. C., and Cloutier, P. A.: 1995, *J. Geophys. Res.* **100**(A12), 23,973.

Lillis, R. J., Mitchell, D. L., Lin, R. P., Connerney, J. E. P., and Acuña, M.H.: 2004, *Geophys. Res. Lett.* **31**(15), L15702, doi: 10.1029/2004GL020189.

Lillis, R. J., Engel, J. H., Mitchell, D. L., Brain, D. A., Lin, R. P., Bougher, S. W., *et al.*: 2005, *Geophys. Res. Lett.* **32**(23), L23204, doi: 10.1029/2005GL024337.

Luhmann, J. G., Russell, C. T., Brace, L. H., and Vaisberg, O. L.: 1992, *Mars, Univ. Arizona press, chap The Intrinsic Magnetic Field and Solar-Wind Interaction of Mars*, p. 1090.

Luhmann, J. G., Acuña, M. H., Purucker, M., Russell, C. T., and Lyon, J. G.: 2002, *Planet Space Sci.* **50**, 489.

Lundin, R., Borg, H., Hultqvist, B., Zakharov, A., and Pellinen, R.: 1989, *Nature* **341**, 609.

Lundin, R., Barabash, S., Andersson, H., Holmström, M., Grigoriev, A., Yamauchi, M., *et al.*: 2004, *Science* **305**, 1933.

Lundin, R., Winningham, D., Barabash, S., Frahm, M., Holmström, R., Sauvaud, J. A., *et al*.: 2005, *Science* **311**(5763), L23204, doi: 10.1126/science.1122071.

Ma, Y., Nagy, A. F., Hansen, K. C., DeZeeuw, D. L., and Gombosi, T. I.: 2002, *J. Geophys. Res.* **107**(A10), 1282, doi: 10.1029/2002JA009293.

Ma, Y., Nagy, A. F., Sokolov, I. V., and Hansen, K. C.: 2004, *J. Geophys. Res.* **109**, A07211, doi: 10.1029/2003JA010367.

Mazelle, C., Winterhalter, D., Sauer, K., Trotignon, J. G., Acuña, M. H., Baumgärtel, K., *et al*.: 2004, *Space Sci. Rev.* **111**, 115.

Mendillo, M., Smith, S., Wroten, J., Rishbeth, H., and Hinson, D.: 2003, *J. Geophys. Res.* **108**(A12), a432, doi: 10.1029/2003JA009961.

Mendillo, M., Withers, P., Hinson, D., Rishbeth, H., and Reinisch, B.: 2006, *Science* **311**(5764), 1135–1138, doi: 10.1126/science.1122099.

Mitchell, D. L., Lin, R. P., Rème, H., Crider, D. H., Cloutier, P. A., Connerney, J. E. P., *et al*.: 2000, *Geophys. Res. Lett.* **27**(13), 1871.

Mitchell, D. L., Lin, R. P., Mazelle, C., Rème, H., Cloutier, P. A., Connerney, J. E. P., *et al*.: 2001a, *J. Geophys. Res.* **106**(E10), 23,419.

Mitchell, D. L., Lin, R. P., Rème, H., Cloutier, P. A., Connerney, J. E. P., Acuña, M. H., *et al*.: 2001b, Probing Mars' crustal magnetic field with the MGS Electron Reflectometer. AGU Spring Meeting Abstracts, pp GP22A–07.

Mitchell, D. L., Lillis, R. J., Lin, R. P., Connerney, J. E. P., and Acuña, M. H.: 2006, *J. Geophys. Res.* in press.

Möhlmann, D., Riedler, W., Rustenbach, J., Schwingenschuh, K., Kurths, J., Motschmann, U., *et al*.: 1991, *Planet Space Sci.* **39**(7), 83.

Morgan, D. D., Gurnett, D. A., Kirchner, D. L., Huff, R. L., Brain, D. A., Boynton, W. V., *et al*.: 2006, *Geophys. Res. Lett.* **33**(13), L13202, doi: 10.1029/2006GL026637.

Nagy, A. F., Winterhalter, D., Sauer, K., Cravens, T. E., Brecht, S., Mazelle, C., *et al*.: 2004, *Space Sci. Rev.* **111**(1), 33, doi: 10.1023/B:SPAC.0000032718.47512.92.

Ness, N. F., Acuña, M. H., Connerney, J. E. P., Kliore, A. J., Breus, T. K., Krymskii, A. M., *et al*.: 2000, *J. Geophys. Res.* **105**(A7), 15,991.

Nielsen, E., Wang, X. D., Gurnett, D. A., Kirchner, D. L., Huff, R., Orosei, R., *et al*.: 2006, *J. Geophys. Res.* in press.

Øieroset, M., Mitchell, D. L., Phan, T. D., and Lin, R. P.: 2001, *Geophys. Res. Lett.* **28**(5), 887.

Øieroset, M., Mitchell, D. L., Phan, T. D., Lin, R. P., Crider, D. H., and Acuña, M. H.: 2004, *Space Sci. Rev.* **111**(1), 185.

Orlowski, D. S., and Russell, C. T.: 1995, *Adv. Space Res.* **15**(8/9), 37.

Pedersen, A., Nairn, C., Grard, R., and Schwingenschuh, K.: 1991, *J. Geophys. Res.* **96**(A7), 11,243.

Phillips, J. L., Luhmann, J. G., and Stewart, A. I. F.: 1986, *Geophys. Res. Lett.* **13**(A4), 1047.

Purucker, M., Ravat, D., Frey, H., Voorhies, C., Sabaka, T., and Acuña, M. H.: 2000, *Geophys. Res. Lett* **27**, 2249.

Riedler, W., Möhlman, D., Oraevsky, V. N., Schwingenschuh, K., Yeroshenko, Y., Rustenbach, J., *et al*.: 1989, *Nature* **341**, 604.

Rosenbauer, H., Shutte, N., Apáthy, I., Galeev, A., Gringauz, K., Grünwaldt, H., *et al*.: 1989, *Nature* **341**, 612.

Russell, C. T., Luhmann, J. G., Schwingenschuh, K., Riedler, W., and Yeroshenko, Y.: 1990, *Geophys. Res. Lett.* **17**(6), 897.

Russell, C. T., Mulligan, T., Delva, M., Zhang, T. L., and Schwingenschuh, K.: 1995, *Planet Space Sci.* **43**(7), 875.

Smith, E. J.: 1969, *Advanced Space Experiments, American Astronautical Society*, chap Planetary Magnetic Field Experiments, Tarzana, CA.

Trotignon, J. G., Dubinin, E., Grard, R., Barabash, S., and Lundin, R.: 1996, *J. Geophys. Res.* **101**(A11), 24,965.

Trotignon, J. G., Mazelle, C., Bertucci, C., and Acuña, M. H.: 2006, *Planet Space Sci.* **54**, 357, doi: 10.1016/j.pss.2006.01.003.

Tyler, G. L., Balmino, G., Hinson, D. P., Sjogren, W. L., Smith, D. E., Woo, R. T., *et al.*: 1992, *J. Geophys. Res.* **97**(E5), 7759.

Tyler, G. L., Balmino, G., Hinson, D. P., Sjogren, W. L., Smith, D. E., Simpson, R. A., *et al.*: 2001, *J. Geophys. Res.* **106**(E10), 23,327.

Vennerstrom, S., Olsen, N., Purucker, M., Acuña, M. H., and Cain, J. C.: 2003, *Geophys. Res. Lett.* **30**(7), 1369, doi: 10.1029/2003GL016883.

Verigin, M., Vignes, D., Crider, D., Slavin, J., Acuña, M., Kotova, G., *et al.*: 2004, *Adv. Space Res.* **33**, 2222, doi: 10.1016/S0273-1177(03)00522-2.

Verigin, M. I., Shutte, N. M., Galeev, A. A., Gringauz, K. I., Kotova, G. A., Remizov, A. P., *et al.*: 1991, *Planet Space Sci.* **39**(1–2), 131.

Verigin, M. I., Gringauz, K. I., Kotova, G. A., Remizov, A. P., Shutte, N. M., Rosenbauer, H., *et al.*: 1993, *J. Geophys. Res.* **98**(A2), 1303.

Vignes, D., Acuña, M. H., Connerney, J. E. P., Crider, D. H., Rème, H., and Mazelle, C.: 2000, *Geophys. Res. Lett.* **27**(1), 49.

Vignes, D., Acuña, M. H., Connerney, J. E. P., Crider, D. H., Rème, H., and Mazelle, C.: 2002, *Geophys. Res. Lett.* **29**(9), 1328, doi: 10.1029/2001GL014513.

Vignes, D., Acuña, M. H., Connerney, J. E. P., Crider, D. H., Rème, H., and Mazelle, C.: 2004, *Space Sci. Rev.* **111**(1), 223, doi: 10.1023/B:SPAC.0000032716.21619.f2.

Winningham, J. D., Frahm, R. A., Sharber, J. R., Coates, A. J., Linder, D., Soobiah, Y., *et al.*: 2006, *Icarus* **182**(2), 360, doi: 10.1016/j.icarus.2005.10.033.

Withers, P., Mendillo, M., Rishbeth, H., Hinson, D. P., and Arkani-Hamed, J.: 2005, *Geophys. Res. Lett.* **32**, L16204, doi: 10.1029/2005GL023483.

Zakharov, A. V.: 1992, in: Luhmann, J. G., and Tatrallyay, Pepin R. O. (eds.), *Venus and Mars: Atmospheres, Ionospheres, and Solar Wind Interactions*, AGU, Washington, DC, Geophys. Monogr. Ser., vol. 66, p. 327.